## Squalene accumulation in cholesterol auxotrophic lymphomas prevents oxidative cell death

| | |
|---|---|
| **Citation** | Garcia-Bermudez, Javier et al. "Squalene accumulation in cholesterol auxotrophic lymphomas prevents oxidative cell death." Nature 567 (2019): 118-122 © 2019 The Author(s) |
| **As Published** | 10.1038/s41586-019-0945-5 |
| **Publisher** | Springer Science and Business Media LLC |
| **Version** | Author's final manuscript |
| **Citable link** | https://hdl.handle.net/1721.1/124755 |
| **Terms of Use** | Article is made available in accordance with the publisher's policy and may be subject to US copyright law. Please refer to the publisher's site for terms of use. |

# Squalene accumulation in cholesterol auxotrophic lymphomas prevents oxidative cell death

**Javier Garcia-Bermudez**[1], **Lou Baudrier**[1], **Erol Can Bayraktar**[1], **Yihui Shen**[2], **Konnor La**[1], **Rohiverth Guarecuco**[1], **Burcu Yucel**[1], **Danilo Fiore**[3], **Bernardo Tavora**[1], **Elizaveta Freinkman**[4], **Sze Ham Chan**[4], **Caroline Lewis**[4], **Wei Min**[2], **Giorgio Inghirami**[3], **David M Sabatini**[4,5], and **Kıvanç Birsoy**[1,*]

[1]Laboratory of Metabolic Regulation and Genetics, The Rockefeller University, 1230 York Avenue, New York, NY 10065, USA

[2]Department of Chemistry and Kavli Institute for Brain Science, Columbia University, New York, NY 10027

[3]Department of Pathology and Laboratory Medicine, Weill Cornell Medical College, New York, NY 10065, USA; Department of Molecular Biotechnology and Health Sciences, University of Turin, 10126, Turin, Italy

[4]Whitehead Institute for Biomedical Research, Nine Cambridge Center, Cambridge, Massachusetts 02142, USA

[5]Howard Hughes Medical Institute and Department of Biology, Massachusetts Institute of Technology, Cambridge, Massachusetts 02139, USA; The David H. Koch Institute for Integrative Cancer Research at MIT, 77 Massachusetts Avenue, Cambridge, Massachusetts 02139, USA; Department of Biology, Massachusetts Institute of Technology (MIT), Cambridge, Massachusetts 02139, USA; Broad Institute of Harvard and MIT, Seven Cambridge Center, Cambridge, Massachusetts 02142, USA.

## Abstract

Cholesterol is essential for cells to grow and proliferate. While normal mammalian cells meet their need for cholesterol through its uptake or *de novo* synthesis[1], the extent to which cancer cells rely

on each of these pathways remains poorly understood. Here, using a competitive proliferation assay on a pooled collection of DNA-barcoded cell lines, we identified a subset that is auxotrophic for cholesterol and thus highly dependent on its uptake. Metabolic gene expression analysis pinpointed loss of squalene monooxygenase (SQLE) expression as a cause of the cholesterol auxotrophy, particularly in ALK+ anaplastic large cell lymphoma (ALCL) cell lines and primary tumors. SQLE catalyzes the oxidation of squalene to 2,3-oxidosqualene in the cholesterol synthesis pathway and its loss results in accumulation of the upstream metabolite squalene, which is normally undetectable. In ALK+ ALCLs, squalene alters the cellular lipid profile and protects cancer cells from ferroptotic cell death, providing a growth advantage under conditions of oxidative stress and in tumor xenografts. Finally, a CRISPR-based genetic screen identified cholesterol uptake by the low-density lipoprotein receptor (LDLR) as essential for the growth of ALCL cells in culture and as patient-derived xenografts. This work reveals that the cholesterol auxotrophy of ALCLs is a targetable liability, and, more broadly, that systematic approaches are useful for identifying nutrient dependencies unique to individual cancer types.

---

Cancer cells can be auxotrophic for specific nutrients due to mutations or decreased expression of metabolic genes[2,3]. The resulting nutrient dependencies provide potential anti-cancer therapies, with the treatment of leukemias with L-asparaginase as the clearest example[3]. Beyond conferring a nutrient dependency, loss of the activity of a metabolic enzyme can also have dramatic effects on the levels of intermediate metabolites, which may in turn impact non-metabolic cellular processes[4–6]. Therefore, the identification of cancer nutrient auxotrophies can both inform the development of future therapies and also elucidate secondary roles for metabolites.

Cholesterol is a cell non-essential nutrient because, in addition to being taken up from the environment, it can be synthesized *de novo* from acetyl-CoA (Fig. 1a). While cholesterol auxotrophy is an exceedingly rare phenotypic trait in normal diploid cells[7,8], some cancer cell lines are known to depend on exogenous cholesterol for their growth. For example, the histiocytic lymphoma cell line U-937 is cholesterol auxotrophic due to a defect in 3-ketosteroid reductase (*HSD17B7*)[7]. When incubated in a lipoprotein-depleted serum, U-937 cells die after four days unless supplemented with cholesterol (Fig. 1b, Extended Data Fig. 1a). To determine whether similar cholesterol dependencies are observed in additional cancer cell lines, we undertook a competitive proliferation assay with a pooled collection of 28 cancer cell lines, each marked with a lentivirally transduced DNA barcode (Fig. 1c). As lipoproteins are the major carriers of cholesterol in human serum[9], the pooled population of cell lines was cultured in lipoprotein-replete or -depleted medium for three weeks. Interestingly, the absence of lipoproteins did not impact the proliferation of most cell lines, suggesting that most can obtain sufficient cholesterol through de novo synthesis (Fig. 1d, Extended Data Fig. 1b,c, Supplementary Table 1). However, lipoprotein depletion did strongly reduce the proliferation of a subset of cancer cell lines, not only U-937, but also U266B1, Raji, Jiyoye and SNU-1, cell lines previously unknown to be sensitive to lipoprotein depletion (Fig. 1d,e). In individual growth assays, these cells can proliferate in lipoprotein-depleted conditions when supplemented with free cholesterol, arguing against an essential role for other components of lipoproteins (Extended Data Fig. 1c,d). These data

demonstrate that strong extracellular cholesterol dependencies can exist in cancer cells of distinct origins.

Cholesterol biosynthesis occurs through a pathway of over thirty successive steps that converts acetyl-CoA to squalene, which is then cyclized into lanosterol and other downstream sterol compounds[1]. While oncogenic alterations may reprogram cholesterol metabolism in a subset of cancers[10], the presence or absence of such mutations did not correlate with differences in the sensitivity to cholesterol depletion (Extended Data Fig. 1e). We therefore considered that a defect in a cholesterol synthesis gene might render these cells auxotrophic for cholesterol. Analysis of transcriptome-wide gene expression data from the Cancer Cell Line Encyclopedia (CCLE) revealed that one of the cholesterol dependent cell lines, SNU-1, does not express squalene monooxygenase (SQLE) mRNA and protein (Fig. 2a, Extended Data Fig. 1f,g). Consistent with a block in the SQLE-catalyzed step of cholesterol biosynthesis, expression of SQLE was sufficient to enable the proliferation of SNU-1 cells under cholesterol depleted conditions (Fig. 2b, Extended Data Fig.1h). SQLE catalyzes the conversion of squalene to squalene-2,3-epoxide and is a rate-limiting step in sterol synthesis in mammalian cells (Extended Data Fig. 1i)[11]. Although squalene, the upstream metabolite in this reaction, is undetectable in most cancer and normal cells, lack of SQLE expression results in accumulation of squalene in SNU-1 cells, further validating the absence of SQLE activity (Fig. 2c). Thus, the SNU-1 cell line is a bona fide cholesterol auxotroph because of its lack of SQLE activity.

Using gene expression data from the CCLE we identified nine additional cell lines without detectable SQLE mRNA and protein. Remarkably, six of these cell lines (SU-DHL-1, KIJK, SUP-M2, DEL, SR-786 and Karpas 299) belong to a specific cancer subtype, Anaplastic Lymphoma Kinase positive (ALK+) anaplastic large cell lymphomas (ALCL) (Fig. 2d,e). Similar to SNU-1, SQLE-deficient ALCL cell lines are sensitive to cholesterol depletion (Fig. 2f) and accumulate high amounts of squalene (Fig. 2g). Chemical imaging using stimulated Raman scattering (SRS) microscopy further revealed that, while control cells lack squalene, ALCLs accumulate it in lipid droplets (Fig. 2h, Extended Data Fig. 2a,b). Loss of SQLE expression is associated with promoter hypermethylation, and treatment with DNA-hypomethylating agents upregulates SQLE mRNA expression (Extended Data Fig. 2c-e). We next investigated whether SQLE downregulation is also a feature of primary tumor samples and patient-derived tumor xenografts of ALK+ ALCLs. Analysis of previously published mRNA expression data from ALCLs[12] and quantitative PCR of primary tumor samples revealed that SQLE is indeed one of the most significantly differentially expressed genes in primary ALK+ ALCL tumors compared to ALK- ALCLs (Fig. 2i, Extended Data Fig. 3a,b, Supplementary Table 2). In agreement with the mRNA data, we observed a marked reduction of SQLE protein levels in primary ALK+ ALCL tumors compared to other lymphoma types (Extended Data Fig. 3c-e). Despite highly significant inverse correlation between NPM-ALK translocation and SQLE expression, modulation of ALK signaling did not affect SQLE expression, suggesting that SQLE may be silenced due to a different mechanism (Extended Data Fig. 3f-h). Altogether, these results demonstrate that ALK+ ALCLs lack SQLE expression and thus are cholesterol auxotrophs.

Given the strong cholesterol dependency of ALK+ ALCLs, we next explored whether this unexpected metabolic feature could be exploited as a therapeutic vulnerability. Using a focused CRISPR library targeting 200 core metabolic enzymes (Supplementary Table 3), we performed a negative selection screen to identify genes whose loss inhibits the fitness of cholesterol auxotrophic ALK+ ALCL cells but not of their SQLE-expressing counterparts or a prototrophic cell line (Fig. 3a, Extended Data Fig. 4a). The highest scoring gene in these screens was the low-density lipoprotein receptor (*LDLR*) (Fig. 3b, Extended Data Fig. 4b-d, Supplementary Table 4). LDLR provides a major source of cholesterol for mammalian cells by serving as the cell surface receptor for the endocytosis of cholesterol-rich LDL[1,9]. Consistent with the screen results and the essential role of LDLR in the survival of ALCLs, depletion of LDLR using a conditional CRISPR-Cas9 system (Fig. 3c, Extended Data Fig. 4e-i) or targeting it with a monoclonal anti-LDLR antibody (Extended Data Fig. 4j-l) strongly decreased the proliferation of ALK+ ALCL lines but not of control cells. ALK+ ALCLs upregulate LDLR-mediated cholesterol uptake (Extended Data Fig. 5a) and expression of cholesterol uptake genes (Fig. 2d, Extended Data Fig. 5b-e) to compensate for their deficiency in *de novo* cholesterol biosynthesis, an adaptation essential for ALK+ ALCL cells to proliferate. Consistent with these findings, CRISPR-Cas9 mediated LDLR depletion inhibited the growth of mouse tumor xenografts derived from ALK+ ALCL cancer cell lines (DEL and Karpas 299) but not that of a control cell line (KMS-26) (Fig. 2e). To translate our findings to a more relevant *in vivo* model, we asked whether targeting LDLR affects the growth of patient-derived xenografts (PDXs). For this, we performed an *in vivo* loss-of-function competition assay using a pool of sgRNAs targeting control genomic regions or the *LDLR* gene. Remarkably, the sgRNAs targeting the *LDLR* gene strongly inhibited the growth of tumors derived from the DEL cell line as well as from three different ALK+ ALCL PDXs, but not that of isogenic tumors expressing SQLE (Fig. 3f). Collectively, our data identify cholesterol uptake via LDLR as a therapeutic target for ALK+ ALCLs *in vivo*.

We reasoned that a decrease in cholesterol synthesis was unlikely to confer an advantage to cancer cells and so investigated whether loss of SQLE activity might have other beneficial effects on ALCL metabolism and growth. As the accumulation of certain metabolites in cancer cells can promote tumorigenesis by altering cellular processes distinct from the original metabolic pathways in question[4,6,13], we focused our attention on squalene, a relatively poorly characterized metabolic intermediate that accumulates at very high levels upon SQLE loss (Fig. 2g). Squalene is a main component of human sebum and proposed to have a role as an emollient and a natural antioxidant for the skin, but the role of squalene in cancer biology has been poorly explored[14,15]. To understand the metabolic consequences of squalene accumulation in ALCLs, we genetically targeted squalene synthase (*FDFT1*), the enzyme immediately upstream of SQLE in cholesterol biosynthesis responsible for the synthesis of squalene. CRISPR-Cas9 mediated knock out of FDFT1 blocked squalene synthesis, and returned squalene to levels seen in non-ALCL cells (Fig.4a,b; Extended Data Fig. 6a,b). To test whether squalene accumulation in ALK+ lymphomas is beneficial for tumor formation *in vivo*, we generated tumors by injecting FDFT1 knock out Karpas 299 cells expressing a vector or an sgRNA resistant FDFT1 cDNA subcutaneously into immunodeficient mice. Loss of FDFT1 caused a marked decrease in the size of Karpas 299 tumors (Fig. 4c). Similarly, competition experiments using FDFT1 and control sgRNAs in

two ALK+ PDX models showed a significant depletion of sgFDFT1 sgRNAs (Extended Data Fig. 6c). These data suggest that squalene synthesis may be beneficial for optimal growth of ALK+ ALCLs *in vivo*.

We next investigated how squalene may impact cellular metabolism in ALK+ ALCLs. As accumulation of lipid peroxides are detrimental to cell viability, most mammalian cells repair lipid damage using the phospholipid peroxidase glutathione peroxidase 4 (GPX4), inhibition of which causes ferroptosis, a recently described form of cell death[16–18]. Squalene is a lipophilic metabolite that can accumulate in cellular membranes and lipid droplets (Fig. 2h, Extended Data Fig. 2b). We therefore asked whether squalene may be protective of lipid peroxidation and ferroptotic cell death. Remarkably, blocking squalene accumulation by genetic loss of *FDFT1* (Fig. 4d, Extended Data Fig. 6d-g), or small molecule inhibitors (Extended Data Fig. 7) sensitized SQLE-deficient cells to ferroptosis induced by GPX4 inhibitors (ML162 and RSL3). Extracellular squalene supplementation fails to provide this protective phenotype, suggesting that squalene may need to accumulate in the right cellular compartments for its function (Extended Data Fig. 8). Consistent with cell death by ferroptosis, the addition of an antioxidant (ferrostatin-1) or blocking long chain PUFA incorporation into membrane lipids by knocking out acyl-CoA synthetase long-chain family member 4 (*ACSL4*)[19] eliminated the sensitivity of FDFT1 KO ALCLs to GPX4 inhibitors (Fig. 4d, Extended Data Fig. 9a-c). Similarly, expression of SQLE cDNA in ALCL cells decreased squalene levels, sensitized them to GPX4 inhibitors and blunted their *in vivo* tumor growth (Fig. 4b-d, Extended Data Fig. 6a,d,e). Additionally, a decrease in squalene levels upon FDFT1 loss or SQLE overexpression increased lipid ROS, a hallmark of ferroptosis rescued by antioxidants when cells were treated with ferroptosis inducers (Extended Data Fig. 9d,e). As membrane PUFAs are highly susceptible to damage by oxidation[19], squalene accumulation may protect these membrane lipids from chemical modification or rewire membrane lipid composition, thereby providing a survival advantage to them under oxidative stress. Reflective of the protective role of squalene, loss of squalene accumulation enhanced the depletion of membrane PUFAs containing arachidonic acid (AA, 20:4), adrenic acid (AdA, 22:4) and docosahexaenoic acid (DHA, 22:6) in FDFT1 null cells upon ML162 treatment (Fig. 4e, Extended Data Fig. 10a-c). While an increase in the levels of GPX4 protein or coenzyme Q[20,21] by inhibition of lower sterol synthesis pathway can protect against lipid peroxidation (Extended Data Fig. 10d), we did not observe a change in GPX4 protein or coenzyme Q in ALK+ ALCLs upon FDFT1 loss (Extended Data Fig. 7,10e-f). Therefore, our findings reveal squalene as a lipophilic metabolite that is elevated in ALK+ ALCLs and can prevent damage of membrane PUFAs under oxidative stress.

Cancer-associated alterations in metabolic enzymes influence the levels of metabolic intermediates and may thereby impact non-metabolic cellular functions such as signaling and the epigenetic state[5,13]. For example, succinate and fumarate accumulate in cancers with SDH or FH mutations and may exert their pro-tumorigenic effects by acting as epigenetic modulators[22,23]. Here, we find that ALK+ ALCLs lose squalene monooxygenase activity and accumulate squalene, a metabolite with antioxidant-like properties (Fig. 4f). As activation of cellular antioxidant defenses is selected for in some tumor types[24] or under certain stresses[21,25,26] and may protect cancer cells from ferroptosis[27], SQLE suppression may be an additional mechanism underlying this cancer hallmark. Future work is required to

understand the role of squalene accumulation in cancer initiation and progression. Additionally, our work identifies cholesterol auxotrophy of ALK+ ALCLs as a targetable metabolic liability and adds ALCLs to the small list of cancers that are selectively auxotrophic for a particular nutrient. As a block in LDL uptake inhibits the growth of ALCL tumors in our pre-clinical PDX models, inhibitors of LDLR, or approaches that decrease serum cholesterol without increasing tumor LDLR levels, might have value in the clinic[28]. Lastly, the workflow we describe can serve as a generalizable approach for identifying additional nutrient dependencies and protumorigenic metabolites across cancer types.

## MATERIAL AND METHODS

### Cell lines, compounds and constructs

Antibodies to SQLE were purchased from ProteinTech (12544–1-AP, immunoblotting) and Atlas Antibodies (HPA020762, immunohistochemistry). Beta-Actin (GTX109639), ACSL4 (GTX100260) and GAPDH (GTX627408) antibodies were obtained from GeneTex; LDL receptor (ab52818), NPC1 (ab36983) and GPX4 (ab41787) antibodies from Abcam; FDFT1 antibody from Protein Tech (13128–1-AP); and ALK (C26G7), STAT3 (9132), phospho-STAT3 (9131) and Histone H3 (4499) antibodies from CST.

HRP-conjugated anti-rabbit antibody was purchased from Santa Cruz; mouse IgG1 isotype control antibody from BioCell; Matrigel from Corning; fetal bovine serum, polybrene, puromycin, squalene and cholesterol from Sigma; blasticidin from Invivogen; low density lipoprotein (LDL) from Lee BioSolutions; oleic acid from Santa Cruz; and Dil-LDL, DAPI and BODIPY 581/591 C11 from Thermo Fisher Scientific.

NB-598 Maleate was obtained from Adooq Bioscience; ML162 from Aobious; erastin from Tocris; RSL3 from Selleckchem; zaragozic acid A (ZA) from Cayman Chemical; Ferrostatin-1 from Abcam; 4-nitrobenzoate from Alfa Aesar; crizotinib, atorvastatin`, 5-azacytidine and 5-Aza-2′-deoxycytidine (Decitabine) from Sigma; and Shield-1 from CheminPharma.

Cell culture images were taken with a REVOLVE4 microscope (Echo Laboratories).

All cell lines used in this study were purchased from ATCC and DSMZ or a gift of Sabatini and Weinberg labs. The identities of all the cell lines used in this study were authenticated by single tandem repeat (STR) profiling. All the cell lines were routinely tested for mycoplasma contamination every two months. Among all the cell lines, two of them were in ICLAC as misidentified cell lines but included in our analysis for diversity due to their oncogene status and metabolic phenotypes: U-937 is a rare histiocytic lymphoma cell line described as auxotrophic for cholesterol, and NCI-H929 is a myeloma cell line with low GLUT3 expression.

All cell lines were cultured in RPMI media (Gibco) containing 1 mM glutamine, 10% fetal bovine serum, penicillin and streptomycin. For proliferation experiments in the absence of serum lipoproteins, regular RPMI was supplemented with 10% Fetal Bovine Lipoprotein

Deficient Serum (LPDS), obtained from Kalen Biomedical. For tracing experiments, [U-$^{13}$C]-Sodium Acetate (Cambridge Isotope Laboratories, CLM-156) was used.

For generation of the lentiviral knockout constructs, annealed oligos (below) were cloned into lentiCRISPR-v2 vector or an inducible DD-Cas9 lentiviral plasmid[29] using a T4 ligase (NEB).

sgACSL4_3F, caccgAATGACAAGCCAAACCCCAG;

sgACSL4_3R, aaacCTGGGGTTTGGCTTGTCATTc;

sgCTRL_1F, caccgAACGTTGGCACTACTTCAC;

sgCTRL_1R, aaacGTGAAGTAGTGCCAACGTTC;

sgCTRL_2F, caccgTCGTGCGCTTCCGGCGGTA;

sgCTRL_2R, aaacTACCGCCGGAAGCGCACGAC;

sgCTRL_3F, caccgTGCCGAGTAATAACGCGAG;

sgCTRL_3R, aaacCTCGCGTTATTACTCGGCAC;

sgCTRL_4F, caccgGTAGGACCTCACGGCGCGC;

sgCTRL_4R, aaacGCGCGCCGTGAGGTCCTACC;

sgCTRL_5F, caccgCGGATTAGAGGTAATGCGG;

sgCTRL_5R, aaacCCGCATTACCTCTAATCCGC;

sgLDLR_2F, caccGGTGAAGAAGAGGTAGGCGA;

sgLDLR_2R, aaacTCGCCTACCTCTTCTTCACC;

sgLDLR_3F, caccGCTGCGAGCATGGGGCCCTG;

sgLDLR_3R, aaacCAGGGCCCCATGCTCGCAGC;

sgLDLR_4F, caccgCCTGGGGCTGGAAATTGCGC;

sgLDLR_4R, aaacGCGCAATTTCCAGCCCCAGGc;

sgLDLR_5F, caccGTGGCCCAGCGAAGATGCGA;

sgLDLR_5R, aaacTCGCATCTTCGCTGGGCCAC;

sgFDFT1_3F, caccGGTGCTGGAGGACTTCCCAA;

sgFDFT1_3R, aaacTTGGGAAGTCCTCCAGCACC;

sgFDFT1_5F, caccgCCGGAGAATGGGCATTGGGA;

sgFDFT1_5R, aaacTCCCAATGCCCATTCTCCGGc;

sgFDFT1_7F, caccGCGGAAGGTGATGCCCAAGA;

sgFDFT1_7R, aaacTCTTGGGCATCACCTTCCGC;

sgFDFT1_8F, caccGTTCATGGAGAGCAAGGAGA;

sgFDFT1_8R, aaacTCTCCTTGCTCTCCATGAAC;

sgFDFT1_10F, caccGACTATCTGGAAGACCAGCA;

sgFDFT1_10R, aaacTGCTGGTCTTCCAGATAGTC;

sgAAVS1_F, caccgGGGCCACTAGGGACAGGAT;

sgAAVS1_R, aaacATCCTGTCCCTAGTGGCCCC;

sgSQLE_5F, caccGCAGCTGTGCTTTCCAGAGA;

sgSQLE_5R, aaacTCTCTGGAAAGCACAGCTGC.

SQLE cDNA and sgRNA-resistant FDFT1 cDNA were synthesized as gBlock (IDT) and cloned into PMXS-IRES-Blast vector by Gibson assembly. HSD17B7 was cloned using the following primers: HSD17B7_F, atggatccgccaccatgcgaaaggtggttttgatcaccgg;

HSD17B7_R, atgcggccgcttataggcatgagccactgagcctgg.

Cloning of oncogenic NPM-ALK into PMXS-IRES-Blast by Gibson assembly was achieved by PCR of wild type NPM-ALK or its dead kinase version from previously generated constructs[30] using the following primers:

NPM-ALK_F,
GCCGGATCTAGCTAGTTAATTAAGCCACCGCCACCATGGAAGATTCGATGGACATG
G;

NPM-ALK_R, GGGCGGAATTTACGTAGCTCAGGGCCCAGGCTGGTTCATG.

## Proliferation Assays

Cell lines were cultured in 96-well plates at 5,000 cells per well in a final volume of 0.2 ml RPMI-1640 media (Gibco) with the indicated treatments. After 5 days of growth, 40 μl of Cell Titer Glo reagent (Promega) was added and luminescence was read using a SpectraMax M3 plate reader (Molecular Devices). Data is presented as relative fold change in luminescence to that of untreated cells. For proliferation assays under lipoprotein depletion, RPMI media was supplemented with 10% LPDS and luminescence was read after 6 days of growth. Data is presented as relative fold change in luminescence to that of cells grown in LPDS media supplemented with 100 ug/mL LDL. In cholesterol rescue experiments, 100ug/ml LDL (corresponding to total 50 ug/mL of cholesterol) or 10 ug/ml free cholesterol were used, as higher free cholesterol levels impair viability of cell lines.

Of note, in our proliferation assays, we observed that glutamine levels, which correlate with the freshness of the culture media, impact the dose of ML162 required to reduce cell proliferation and viability.

## Real Time PCR assays

RNA was isolated by an RNeasy Kit (Qiagen) according to the manufacturer's protocol. RNA was spectrophotometrically quantified and equal amounts were used for cDNA synthesis with the Superscript II RT Kit (Invitrogen). qPCR analysis was performed on an ABI Real Time PCR System (Applied Biosystems) with the SYBR green Mastermix (Applied Biosystems). The primers used are: hSQLE-F, tccttgctcaggctctttatg; hSQLE-R, agggttaggagacaatacagaaag; HSD17B7-F,gacctttgagtgtggctttg; HSD17B7-R, acggaggcagaattccatatg; RPLO-F, cctctttcccttcggtgtg; RPL0-R, aatcttggcatcagggacac; NPM-F, gggccagtgcatattagtgga; ALK-R, tgtactcagggctctgcagct; hACTINB-F, ttttggctataccctactggca; hACTINB-R, ctgcacagtcgtcagcatatc; mSQLE-F, cccaaaacacaaaatcctcag; mSQLE-R, gcaatgccaagaaaagtccac; mACTINB-F, gttgtgaatgtattggctcagg; mACTINB-R, aatattgaaagcaacccaacagg. Results were normalized to RPL0 or ACTINB.

## Dil-LDL Uptake

Cells were washed twice in HBSS (Gibco) and resuspended (250,000 cells/replicate) in 0.5 mL of LPDS media supplemented with 5 ug/mL of Dil-LDL. To measure nonspecific emission, one control well was used by adding 5 ug/mL of non-fluorescent unlabeled LDL. Cells were incubated at 37 °C for 6 hrs prior to collection in 1.5 mL tubes and two consecutive washes with HBSS. Cells were then lysed with 100 uL of radioimmunoprecipitation assay (RIPA) buffer and spun down for 5 min at 20,000g. 50 uL of the supernatants were transferred to a 96-well plate (Greiner) and fluorescence was measured with a SpectraMax M3 plate reader at an excitation wavelength of 520 nm and an emission wavelength of 580 nm. Dil-LDL uptake is shown as the specific Dil-LDL emission at 580 nm per ug of protein.

## Generation of Knockout and cDNA Overexpression Cell Lines

For inducible knockout experiments, sgRNAs targeting LDLR (GCTGCGAGCATGGGGCCCTG), ACSL4 (GAATGACAAGCCAAACCCCAG) or a control sgRNA (AAVS1, GGGGCCACTAGGGACAGGAT) were cloned into lentiviral DD-Cas9 vector. This vector was transfected into HEK293T cells with lentiviral packaging vectors VSV-G and Delta-VPR using XtremeGene transfection reagent (Roche). For transduction, indicated cells were spin-infected in 6-well tissue culture plates using 8 μg/ml of polybrene at 2,200 rpm for 1.5 hr and selected by puromycin prior to addition of 250 nM Shield-1 reagent for 3 days. The knockout of the target gene was verified by immunoblotting. For generation of FDFT1-knockout cells or SQLE-knockout cells, an sgRNA targeting FDFT1 (GCCGGAGAATGGGCATTGGGA) or SQLE (GCAGCTGTGCTTTCCAGAGA) was cloned into lentiCRISPR-v2. After transduction and selection using puromycin, cells were single-cell cloned. For overexpression of SQLE, guide-resistant version of FDFT1, NPM-ALK or its dead kinase version, retroviral vectors

with indicated cDNAs were transfected with retroviral packaging plasmids Gag-pol and VSV-G into HEK293T cells. After transduction, cells were selected with blasticidin.

## Metabolite Profiling and Isotope Tracing

For lipid metabolite profiling experiments, each indicated cell line ($1 \times 10^6$ cells per replicate) was cultured as triplicates in 6-well plates and treated for 24 hrs with ML162 (200 nM), Fer-1 (1 uM), ZA (20 uM), 4-NB (1 mM) or Atorvastatin (1 uM) prior to collection of cells and two consecutive washes with 1 mL of cold 0.9% NaCl. To measure squalene synthesis, SNU-1 cells were seeded in 60 mm dishes at 70% confluency. After 24 hours, cells were given fresh medium with [U-$^{13}$C]sodium acetate (10 mM). Cell pellets were resuspended in 600 uL of cold LC/MS grade methanol, and non-polar metabolites extracted by consecutive addition of 300 uL LC/MS grade water followed by 400 uL of LC/MS grade chloroform. After 10 min extraction by vortexing and centrifugation for 10 min at 10,000 × g and $4^{\circ}$C, the lower lipid-containing layer was carefully collected and dried under nitrogen. Dried lipid extracts were stored at $-80^{\circ}$C until LC/MS analysis.

Lipids were separated on an Ascentis Express C18 2.1 × 150mm 2.7 um column (Sigma-Aldrich) connected to a Dionex UlitMate 3000 UPLC system and a QExactive benchtop orbitrap mass spectrometer (Thermo Fisher Scientific) equipped with a heated electrospray ionization (HESI) probe. Dried lipid extracts were reconstituted in 50 uL 65:30:5 acetonitril:isopropanol:water (v/v/v) and 5 uL of sample were injected into the LC/MS/MS, with separate injections for positive and negative ionization modes. Mobile phase A in the chromatographic method consisted of 60:40 water:acetonitrile with 10 mM ammonium formate and 0.1% formic acid, and mobile phase B consisted of 90:10 isopropanol: acetonitrile, with 10 mM ammonium formate and 0.1% formic acid. The chromatographic gradient was described previously[31]. The column oven and autosampler were held at 55 $^{\circ}$C and 4 $^{\circ}$C, respectively. The mass spectrometer parameters were described previously[32]. The spray voltage was set to 4.2 kV, and the heated capillary and the HESI were held at $320^{\circ}$C and $300^{\circ}$C, respectively. The S-lens RF level was set to 50, and the sheath and auxiliary gas were set to 35 and 3 units, respectively. These conditions were held constant for both positive and negative ionization mode acquisitions. External mass calibration was performed every 7 days using the standard calibration mixture.

Mass spectra were acquired in both full-scan and data-dependent MS/MS mode. For the full-scan acquisition, the resolution was set to 70,000, the AGC target was $1\times10^6$, the maximum injection time was 50 msec, and the scan range was $m/z$ = 133.4–2000. For data-dependent MS/MS, the top 10 ions in each full scan were isolated with a 1.0-Da window, fragmented with a step-wise collision energy of 15, 25, and 35 units, and analyzed at a resolution of 17,500 with an AGC target of $2\times10^5$ and a maximum injection time of 100 msec. The underfill ratio was set to 0. The selection of the top 10 ions was set to isotopic exclusion, a dynamic exclusion window of 5.0 sec, and an exclusion list of background ions based on a solvent bank.

High-throughput identification and relative quantification of lipids was performed separately for positive and negative ionization mode data, using LipidSearch software (ThermoFisher Scientific/ Mitsui Knowledge Industries)[33,34] and the default parameters for QExactive

product search and alignment. After alignment, raw peak areas for all identified lipids were exported to Microsoft Excel and filtered according to the following predetermined quality control criteria: Rej ("Reject" parameter calculated by LipidSearch) equal to 0; PQ ("Peak Quality" parameter calculated by LipidSearch software) greater than 0.85; CV (standard deviation/ mean peak area across triplicate injections of a represented (pooled) biological sample) below 0.4; $R$ (linear correlation across a three-point dilution series of the representative (pooled) biological sample) greater than 0.9. Typically, approximately 70% of identified lipids passed all four quality control criteria. Raw peak areas of the filtered lipids were added together to create a total lipid signal for each sample, and individual lipid peak areas were normalized to this total signal as a control for lipid extraction and efficiency, as well as sample loading. Of note, in the total lipid quantification of FDFT1 knockout Karpas299 cells compared to rescued control, we observed an enrichment of membrane phospholipids containing saturated fatty acids (Extended Data Fig. 7c), likely due to the fact that these species are more resistant to oxidative stress and may replace or be enriched in membrane lipids upon oxidative stress.

To measure cholesterol, lanosterol, squalene and CoQ10, a XCalibur QuanBrowser 2.2 (Thermo Fisher Scientific) was used a 5 ppm mass tolerance and referenced an in-house library of chemical standards. Total lipid signal calculated with LipidSearch was used to normalize raw peak areas to generate relative abundance.

### Immunoblotting

Cell pellets were washed twice with ice-cold PBS prior to lysis in lysis buffer (10 mM Tris-Cl pH 7.5, 150 NaCl, 1 mM EDTA, 1% Triton X-100, 2% SDS, CHAPS 0.1%) supplemented with protease inhibitors and PhosSTOP (Roche). Each cell lysate was sonicated and, after centrifugation for 10 min at 4C and 20,000 g, supernatants were collected and their protein concentration determined by a Pierce BCA Protein Assay Kit (Thermo Scientific) with bovine serum albumin as a protein standard. Samples were resolved on 8% or 12% SDS-PAGE gels and analyzed by immunoblotting as previously described[35].

### Targeted bisulfite sequencing

Assays were designed targeting CpG sites in SQLE promoter region using primers created with Rosefinch. All primers were resuspended in TE solution at 100 μM and validated using 1 ng of bisulfite-converted control DNA. Following primer validation, samples were bisulfite converted using the EZ DNA Methylation-LightningTM Kit (Zymo #D5030) according to the manufacturer's instructions. Multiplex amplification of all samples with specific primer pairs and the Fluidigm Access ArrayTM System was performed according to the manufacturer's instructions. The resulting amplicons were pooled for harvesting and subsequent barcoding according to the Fluidigm instrument's guidelines. After barcoding, samples were purified by a ZR-96 DNA Clean & Concentrator (Zymo #D4023) and then prepared for massively parallel sequencing using a MiSeq V2 300bp Reagent Kit and paired-end sequencing protocol according to the manufacturer's guidelines.

Sequence reads were identified by a standard Illumina base-calling software and then analyzed by a Zymo Research proprietary analysis pipeline, which is written in Python. Low quality nucleotides and adapter sequences were trimmed off during analysis QC. Sequence reads were aligned back to the reference genome using Bismark, an aligner optimized for bisulfite sequence data and methylation calling[36]. Paired-end alignment was used as default thus requiring both read 1 and read 2 be aligned within a certain distance, otherwise both read 1 and read 2 were discarded. Index files were constructed using the *bismark_genome_preparation* command and the entire reference genome. The *-- non_directional* parameter was applied while running Bismark. All other parameters were set to default. Nucleotides in primers were trimmed off from amplicons during methylation calling. The methylation level of each sampled cytosine was estimated as the number of reads reporting a C, divided by the total number of reads reporting a C or T.

**DNA-barcode cell mixing**

DNA barcode cell competition assay was performed as previously described using the same primer and barcoding sequences[35] (Supplementary Table 1). Briefly, a unique seven base pair sequence was transduced into 28 different cancer cell lines using lentiviruses produced from a PLKO.1P vector. Each cell line was infected with three barcodes in separate infections for statistical analysis. To perform cell competition assays, barcoded cell lines were mixed in equal amounts and the mixed population was cultured under indicated conditions for 15 days. Cells were then harvested for genomic DNA and processed for Illumina deep sequencing. Barcode abundance was determined in the starting population and after the growth.

**CRISPR-based screen**

The highly focused metabolism sgRNA library was designed as previously described by including representation of key genes of every mammalian metabolic pathway (Supplementary Table 3). Oligonucleotides for sgRNAs were synthesized by Integrated DNA Technologies and annealed prior to be introduced in lentiCRISPR-v2 vector using a T4 DNA ligase kit (NEB) and following manufacturer's instructions. Ligation products were then transformed in NEB stable competent E. coli (NEB) and the resulting colonies were grown overnight at 32 °C and plasmids isolated by Miniprep (QIAGEN). This plasmid pool was used to generate a lentiviral library containing 5 sgRNAs per gene target. This viral supernatant was titered in each cell line by infecting target cells at increasing amounts of virus in the presence of polybrene (8 μg/ml) and by determination of cell survival after 3 days of selection with puromycin. $2 \times 10^6$ of each cell type were infected at a MOI of 1 prior to selection with puromycin for 3 days. An initial pool of 2 million cells was harvested. Infected cells were then cultured for 14 population doublings, after which 2 million cells were collected and their genomic DNA extracted by a DNeasy Blood & Tissue kit (QIAGEN). For amplification of sgRNA inserts, we performed PCR using specific primers for each condition. PCR amplicons were then purified and sequenced on a NextSeq 500 (Illumina). Sequencing reads were mapped and the abundance of each sgRNA was measured. Gene score is defined as the median $\log_2$ fold change in the abundance between the initial and final population of all sgRNAs targeting that gene.

### Immunohistochemistry

Immunohistochemistry staining was performed as previously described[12]. SQLE protein expression was evaluated in Primary and patient-derived tumor xenograft ALCL formalin fixed tissues samples using a rabbit polyclonal anti human SQLE (Atlas Antibodies, 1:200).

### LDLR monoclonal antibody purification

Hybridoma cell lines producing a monoclonal antibody against LDLR was described previously[37]. These cell lines were cultured in RPMI supplemented with 20% FBS and 2 mM pyruvate. LDLR antibody was then purified using a Protein G resin (GenScript) and Protein G Sepharose 4 Fast Flow (GE Healthcare) following manufacturer's instructions.

### C11-Bodipy Lipid peroxidation

Cells were plated (250,000 cells/well) in 6-well plates and treated with ML162 for 18 hrs prior to two washes with HBSS and incubation of cells in 500 uL of HBSS containing BODIPY 581/591 C11 (1 uM). After 15 min incubation at 37 °C, cells were washed twice on ice-cold HBSS and resuspended in 0.5 mL of HBSS containing 50ng/ml DAPI and filtered into FACS tubes with cell-strainer cap (Falcon). Flow cytometry data were collected on a BD LSR II Flow Cytometer (BD Biosciences) by using an excitation wavelength of 488nm and the FL1 collection channel. FlowJo v.10 software was used for data analysis. Live cells were selected from the starting cell population on a DAPI/FSC-A plot. Then, single cells were selected using a FSC-A/FSC-H plot from the population of live cells. Data represents populations of live, singlet cells.

### Spontaneous Raman Spectroscopy and Stimulated Raman Scattering Microscopy

Spontaneous Raman spectra were acquired by a confocal Raman microspectroscopy (Xplora; HORIBA Jobin Yvon) equipped with a 532 nm (40 mW) laser and a 100× objective (air, N.A.=0.9, MPlan N; Olympus). Spectra of pure squalene and cholesterol were acquired with 5 sec integration. Cell spectra were obtained from the lipid droplets (identified under bright field) of cells fixed with 4% paraformaldehyde after 120 sec integration. Glass and solution background was subtracted by measuring signal from adjacent area.

Chemical imaging by Stimulated Raman Scattering Microscopy (SRS) was acquired on an integrated inversed confocal laser-scanning microscope (FV1200; Olympus) equipped with a water-immersion 25× objective (1.05 N.A. XLPLNXWMP2; Olympus). Concentration mapping of selected chemical bond vibration was achieved by raster-scanning two spatially and temporally overlapped picosecond laser beams (picoEmerald, Applied Physics and Electronics) across the sample. SRS signal was generated when the frequency difference of the two beams (pump, tunable; Stokes, 1064nm) matched the vibrational frequency, and was subsequently extracted through high-frequency modulation transfer scheme. Specifically, the Stokes beam was modulated by an electro-optic modulator at 8MHz. Transmitted light was collected by an oil-immersion condenser (1.4 N.A.; Olympus) and filtered by a bandpass filter (890/220 CARS; Chroma Technology), so that only pump beam was detected by a Si photodiode (FDS1010; Thorlabs, biased at 64V). The terminated signal was then pre-filtered (8MHz ± 1MHz, KR 2724; KR electronics), and then demodulated by a lock-in amplifier (SR844; Stanford Research Systems). Laser powers on sample were measured to be 120mW

(Stokes) and 100mW (pump). Images were acquired at a speed of 100s/pixel by Fluoview Software.

Images at three channels were obtained for each cell, and the corresponding wavelengths of pump are: 928.4 nm (1372 cm$^{-1}$), 927.2 nm (1386 cm$^{-1}$), 926.0 nm (1400 cm$^{-1}$). Among these, 1386 cm$^{-1}$ is the squalene on-resonance frequency (vibrational peak), while 1372 cm$^{-1}$ and 1400 cm$^{-1}$ are the squalene off-resonance frequencies (baseline of cell mass). Thus image of squalene distribution is calculated as

$$I_{squalene} = I_{1386} - \left(I_{1372} + I_{1400}\right)/2$$

where $I$ represent SRS intensity from each channel. Images were calculated (in unit of demodulated terminated photocurrent) and later assigned pseudo colors in ImageJ.

SRS signal is proportional to concentration and it is limited by laser shot noise, thus the detection limit is usually submillimolar to millimolar[38]. Squalene accumulates at these high concentrations in lipid droplets, but may still be present in other subcellular compartments and membranes at lower concentrations, but remains undetected by SRS microscopy.

### Gene correlation of primary ALCLs and cancer cell lines

RNAseq data was obtained from a previously published work with SRA accession number SRA176318[12]. Differentially expressed transcripts were identified using the R package limma. False discovery rate was used to correct for multiple hypothesis testing with a significance threshold of 0.01. The identification of most differentially expressed genes was done using the Student t-test statistic (Supplementary Table 2). Microarray expression data of SQLE was obtained from Cancer Cell Line Encyclopedia[39].

### Generation of Patient-Derived Tumor Xenografts

PDX models were described previously[12,40]. Briefly, tumor graft samples were cut into multiple 3×3×1 mm pieces (multiple pieces/specimen) in complete media and implanted fresh and/or cryopreserved in 10% DMSO-RPMI-1640 frozen media supplemented with 20% FCS. Six- to eight-week-old NOD.Cg *B2m*$^{tm1Unc}$ *Prkdc*$^{scid}$ *Il2rg*$^{tm1Wjl}$/SzJ mice (NSG) were first anesthetised (Rompun 0.05µl/g e Zoletil 1.6µg/g i.m.). Then, with animals lying on their ventral site, the dorsal region was sterilized (70% ethanol). Multiple tumorgraft tissue fragments (2–4) were transferred into the subcutaneous using a trocar. Implant growth was assessed by palpation and or by MRI scanning and harvested when tumor masses were required. Tumor volumes were assessed using an electronic caliber. Recipient animals were checked regularly and sacrificed at early sign of distress. At harvesting, mice were sacrificed in a CO2 chamber and grafts were collected for histologic evaluation, re-grafting, or snap-freezing in liquid nitrogen. Tumors were then dissociated to single cells using a phosphate buffer containing Collagenase A (25000 U/mL), Dispase II (12.5 U/mL), DNAse (500 U/mL). Cells were then filtered through a 100um filter and washed twice in PBS. After an overnight culture in RPMI (Lonza), floating live cells were selected with a ficoll (Ficoll-Paque™-Plus, GE Healthcare). Multicolor flow cytometry was used to check the percentage of the neoplastic T-Cells.

Fresh and/or viable cryopreserved samples were obtained at the time of diagnosis, prior treatment, or at relapse after single or multiple chemotherapy protocols. Informed consent was obtained following the procedures approved by the Weill Cornell and Memorial Sloan Cancer ethical committees. Diagnoses were assigned according to the WHO classification by at least two experienced pathologists. Samples IL69 and IL79 (ALK+ PDX1 and ALK+ PDX3 in Fig. 2h) correspond to patients who experience a refractory clinical course unresponsive to standard chemo-immunotherapy. IL69 correspond to a 20-year-old male diagnosed with ALK+ ALCL of the right shoulder, who received 2 cycle of CHOP followed by two additional 3 cycles of BV-CHP. On progressive disease, the patient was treated with Crizotinib but he died with active systemic disease and CNS involvement after a month. IL79 was a 65-year-old male with a relapsed ALK+ ALCL treated with BV-CHOP vs CHOP, who also died with progressive disease after 4 month of therapy (Supplementary Table 5).

### Mini competition assay

Five control sgRNAs targeting intergenic regions, four sgRNAs targeting *LDLR*, and five sgRNAs targeting *FDFT1* were cloned into linearized lentiCRISPR-v2 vector and transformed in NEB competent E. coli. Each plasmid was then pooled at equal concentrations and used for lentivirus production as previously described. DEL cell line was infected and selected with puromycin for 3 days prior to being *in vitro* cultured or injected subcutaneously in NSG mice. Similarly, collagenase digested ALCL patient derived xenograft cells were transduced with the same lentiviral particles and subsequently injected subcutaneously in immunodeficient mice 24 hrs after infection. No antibiotic selection was performed as these cells cannot grow under standard culture conditions. Tumors were collected after 2–4 weeks of growth. An initial pool of each sample was taken for normalization. After 14–21 days gDNAs were isolated and amplified by PCR. PCR amplicons were then sequenced on a NextSeq 500 (Illumina). Guide scores were calculated as median $\log_2$ fold change in the abundance between the initial and final population of that sgRNA similar to standard CRISPR screens.

### Mouse studies

All animal studies and procedures were conducted according to a protocol approved by the Institutional Animal Care and Use Committee (IACUC) at the Rockefeller University. All mice were maintained on a standard light-dark cycle with food and water ad libitum. For *in vivo* LDLR experiments, xenograft tumors were initiated by injecting $1 \times 10^6$ cells/100 uL PBS of ALCL or control cell lines subcutaneously. For ALCL cells coming from patient derived xenografts, injections contained $1 \times 10^6$ cells/100 uL 30% Matrigel. After injections in the left and right flanks of male and female 6–14 weeks old NOD scid gamma (NSG) mice (Taconic), tumors were grown for 2–4 weeks. For patient-derived tumor xenograft models, NSG B2m and NSG mice were handled according to Weill Cornell Medical Institute's Institutional Animal Care and Use Committee-approved protocol #2014–0024. All operatively resected tumors were collected after written patient consent and in accordance with the institutional review board (IRB)–approved protocols of Weill Cornell Medical Institute (2014–0024, 0201005295R012, 1410015560A002 and 0107004999).

For tumor experiments with FDFT1 knock-out and SQLE expressing Karpas299 cell lines, $5–10 \times 10^4$ cells/100 uL PBS of each cell line were injected subcutaneously into NSG mice and grown for 28 days. Injection of higher number of cells resulted in a loss of significance in tumor size difference, a result that is in line with previously published work[26].

In no cases xenograft tumor size surpassed the limit permitted by our protocol (2 cm). All treatment studies were randomized and injections were performed by blinded investigators.

## Statistics and reproducibility

GraphPad PRISM 7 and Microsoft Excel 15.21.1 software were used for statistical analysis. All experiments were performed at least two times with similar results. Both technical and biological replicates were reliably reproduced.

## Extended Data
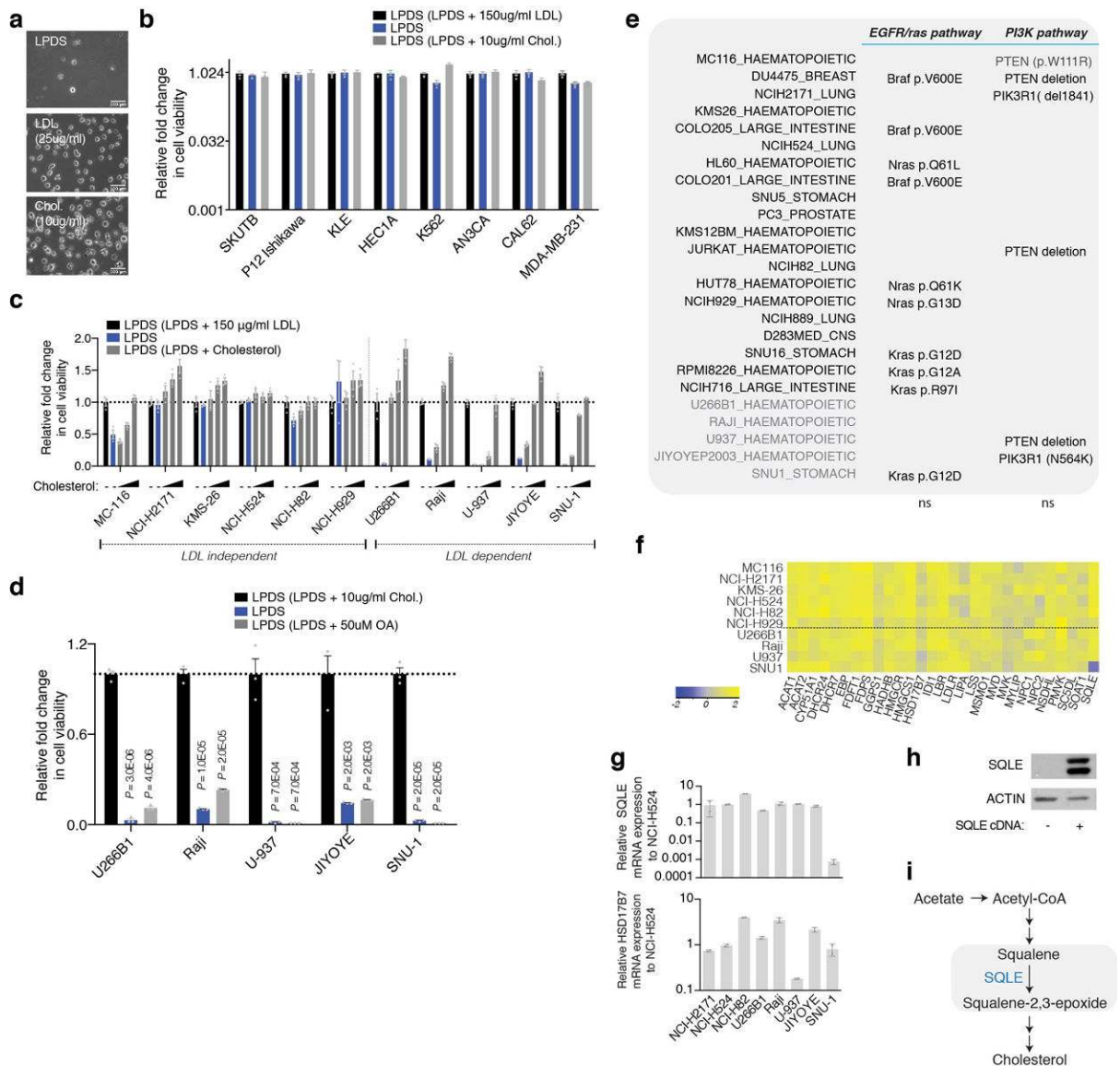


**Extended Data Figure 1. Extracellular cholesterol dependence of cancer cell lines**

**a.** Representative bright-field micrographs of U-937 cells cultured with the indicated concentrations of cholesterol and LDL

**b.** Relative fold change in cell number of indicated cell lines cultured for 5 days with LPDS in the presence or absence of free cholesterol relative to LDL replete serum.

**c.** Relative fold change in cell number of indicated cell lines grown for 5 days under LPDS with or without free cholesterol (1, 5, 10 ug/ml) relative to LDL replete serum.

**d.** Fold change in cell viability of cholesterol auxotrophic cancer cell lines grown for 5 days with LPDS in the presence or absence of cholesterol or oleic acid (OA), relative to LPDS supplemented with free cholesterol.

**e.** Reported alterations in copy number or driver mutations in oncogenic EGFR/Ras and PI3K pathways of cancer cell lines used in the DNA barcode-based competition assay.

**f.** Heatmap showing mRNA expression levels of cholesterol metabolism genes in LDL-dependent and -independent cancer cell lines. Color bar indicates scale (log$_2$ transformed).

**g.** SQLE and HSD17B7 mRNA levels of indicated cell lines relative to cholesterol prototroph cell line NCI-H524. mRNA levels were measured using a real time PCR assay. RPL0 is used as a control.

**h.** Immunoblotting of SQLE in SNU-1 cell lines transduced with a control vector or an SQLE cDNA. Actin is included as a loading control.

**i.** Schematic depicting squalene synthesis from acetate.

In **b**, **c**, **d** and **g**, bars represent mean ± SD. For **b**, **c** and **d**, $n = 3$ biologically independent samples. For **g**, $n = 2$ biologically independent samples. Statistical test used was two-tailed unpaired $t$-test.
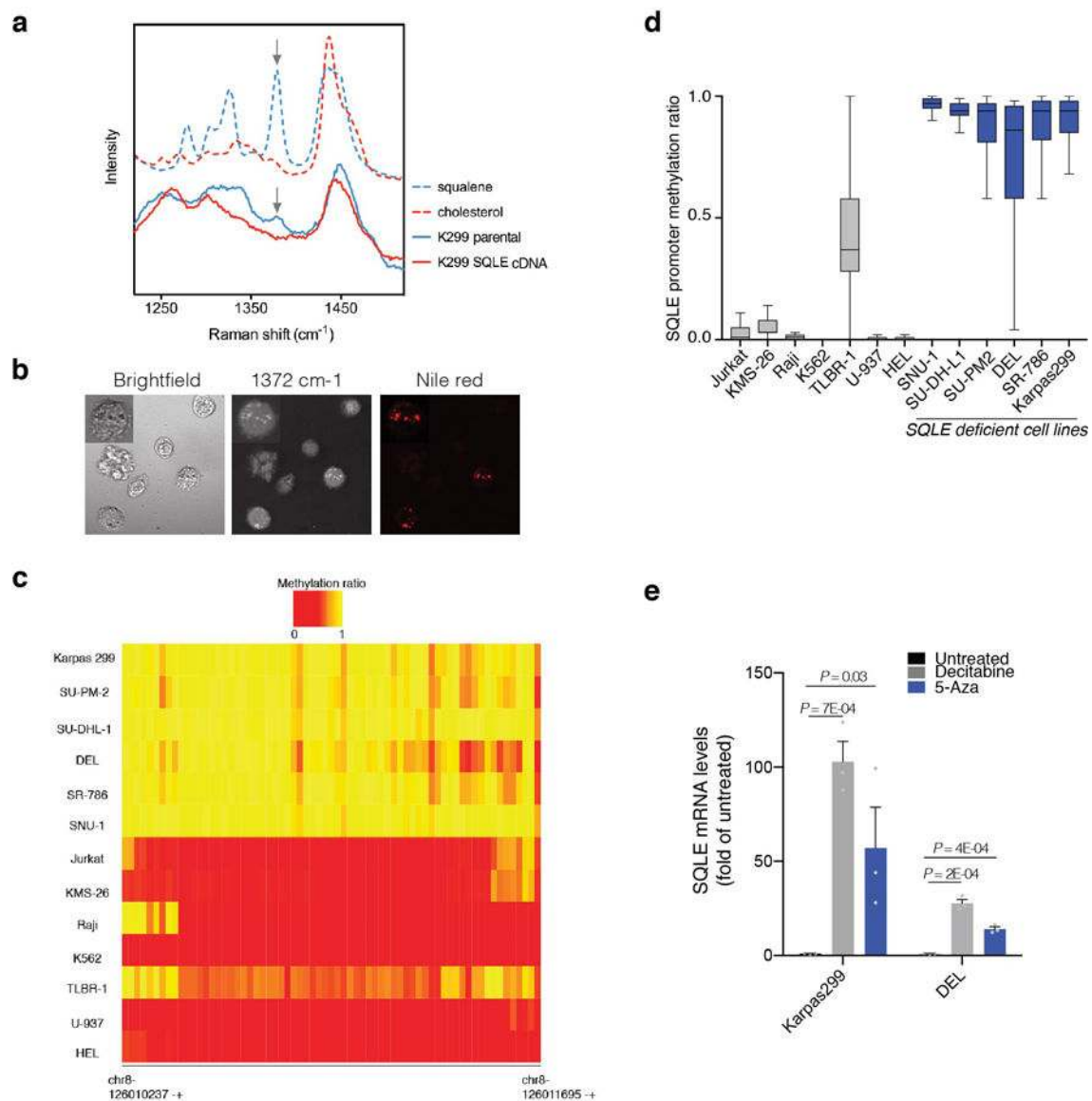


**Extended Data Figure 2. Promoter hypermethylation of the SQLE gene and accumulation of squalene in lipid droplets (LDs) of ALK+ ALCLs**

**a.** Raman spectra of squalene (blue dashed), cholesterol (red dashed), LDs in Karpas299 parental cell (blue solid), and LDs in Karpas299 cell expressing SQLE cDNA (red solid). LDs were identified in bright field and targeted in the confocal Raman microspectrometer. Arrows indicate squalene-specific Raman peak.

**b.** Representative bright field image, SRS image obtained at cell lipid background (1372cm$^{-1}$) and fluorescence of Nile Red staining (for lipid droplets) in Karpas299 cells.

**c.** Heat map showing the DNA methylation ratio for the indicated genomic region containing SQLE promoter for indicated cancer cell lines. Chromosomal position range and strand is indicated. Color bar indicates scale.

**d.** SQLE promoter methylation ratio of control (grey) and SQLE deficient (blue) cancer cell lines. The boxes represent the median and the first and third quartiles, and the whiskers represent the minimum and maximum data points still within 1.5 of the interquartile range ($n$ = 67 independent genomic positions per sample).

**e.** Fold change in SQLE mRNA expression levels of indicated cell lines after treatment with decitabine (500 nM for 4 days) or 5-azacytidine (5-Aza, 1 uM for 6 days), relative to untreated cells (mean ± SD, $n$ = 3 biologically independent samples).
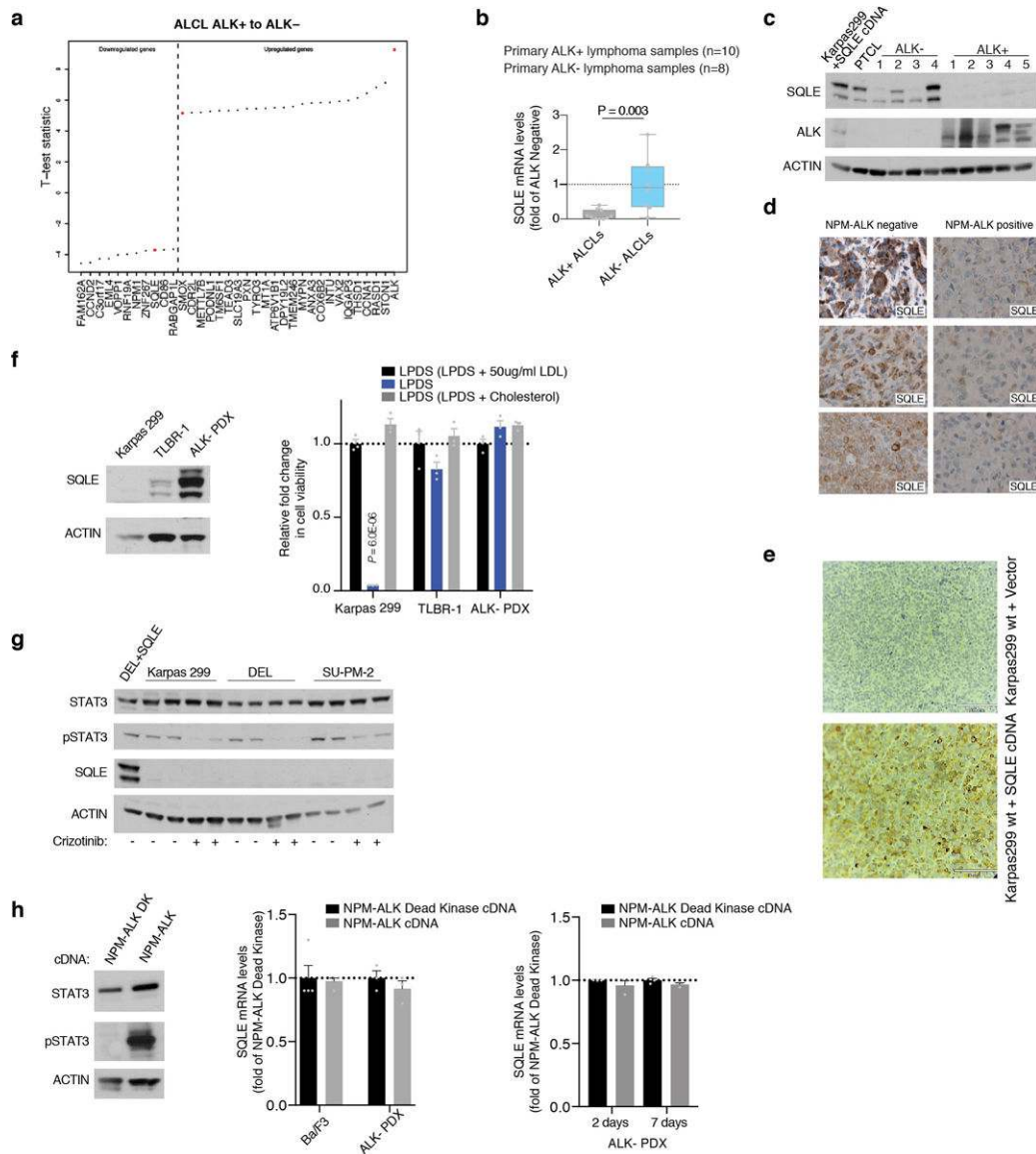
**Extended Data Figure 3. Lack of SQLE expression in primary ALK+ ALCLs**

**a.** List of most up and downregulated genes from differential expression analysis of primary ALK+ primary samples compared to ALK- samples. The student t-test statistic of each gene is calculated and used as a ranking metric ($n = 17$ biologically independent ALK- samples, 5 biologically independent ALK+ samples).

**b.** Fold change in SQLE mRNA expression levels of primary ALK+ ALCLs relative to primary ALK- ALCLs, using ACTIN as a control. The boxes represent the median and the first and third quartiles, and the whiskers represent the minimum and maximum of all data points. Statistics: two-tailed unpaired $t$-test.

**c.** Immunoblotting of SQLE and ALK in indicated patient derived xenograft and cell line models. Actin was used as the loading control. PTCL: Peripheral T-cell Lymphoma.

**d.** Immunohistochemical staining of SQLE in ALK+ and ALK- ALCL primary tumor samples.

**e.** Immunohistochemical staining of SQLE in Karpas299 xenograft tumors transduced with a control or SQLE cDNA. Representative images are shown.

**f.** Immunoblotting of SQLE of indicated cell lines (top). Relative fold change in cell viability of the indicated ALK+ (Karpas299) and ALK- cell lines (TLBR-1 and ALK- PDX cell line) grown for 5 days under LPDS with or without free cholesterol relative to LDL replete serum (bottom) (mean ± SD, $n = 3$ biologically independent samples).

**g.** Immunoblotting of STAT3, phospho-STAT3 and SQLE in indicated cell lines after 72 hrs treatment with crizotinib (200 nM). Actin was used as a loading control.

**h.** Immunoblotting of STAT3 and phospho-STAT3 3 days after transduction of Ba/F3 with a dead kinase version of the NPM-ALK fusion (NPM-ALK DK) or with oncogenic NPM-ALK cDNA.

**i.** SQLE mRNA levels of Ba/F3 and ALK- ALCL cell lines 2 or 7 days after transduction with NPM-ALK DK or NPM-ALK, relative to levels in NPM-ALK DK. mRNA levels were quantified with a real time PCR assay using ACTINB as a control (mean ± SD, $n = 3–4$ biologically independent samples).

In **b**, the boxes represent the median, and the first and third quartiles, and the whiskers represent the minimum and maximum of all data points. In **f** and **h**, bars represent mean ± SD. For **f** and **h**, $n = 3$ biologically independent samples. Statistical test used was two-tailed unpaired $t$-test.
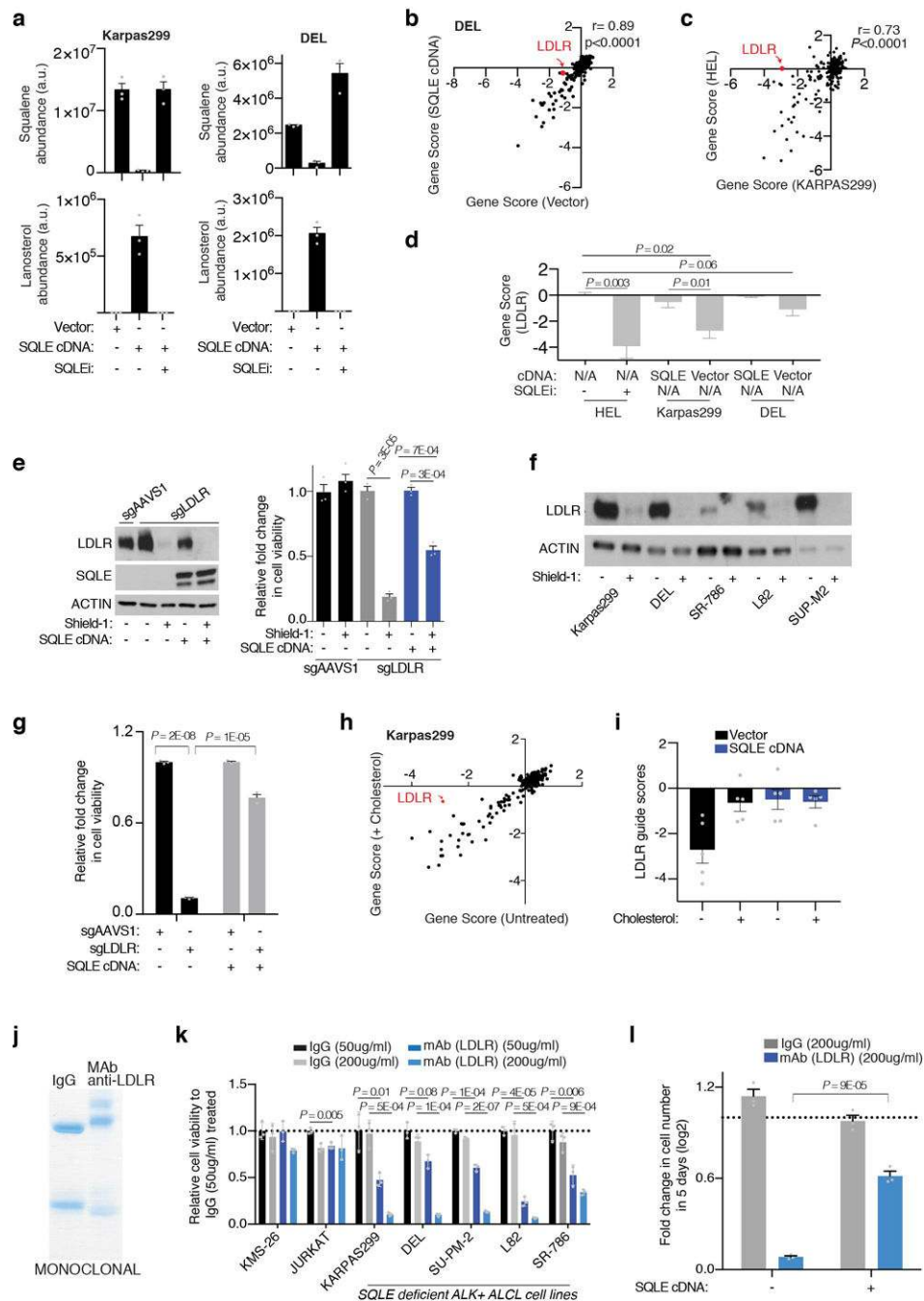
**Extended Data Figure 4. LDLR is an essential gene for the growth of ALK+ ALCLs**

**a.** Squalene and lanosterol abundance of Karpas299 and DEL cell lines in the absence or presence of SQLE cDNA or after incubation for 24 hrs with an SQLE inhibitor (SQLEi, 1 uM).

**b.** Gene essentiality scores for control or SQLE-expressing DEL cell line. Pearson correlation coefficients are indicated. Red dot denotes LDLR.

**c.** Gene essentiality scores for cholesterol-auxotroph Karpas299 or cholesterol-prototroph HEL cell lines. Pearson correlation coefficients are indicated. Red dot denotes LDLR.

**d.** LDLR guide scores of the indicated cell lines in the presence or absence of SQLE inhibitor.

**e.** Immunoblots for LDLR and SQLE in control and SQLE cDNA expressing Karpas299 cells infected with sgAAVS1 or sgLDLR1 virus in the presence or absence of Shield-1 (250 nM) (left). Relative fold change in cell viability of indicated cancer cell lines grown in the absence and presence of Shield-1 for 5 days (right).

**f.** Immunoblotting of LDLR in ALK+ ALCL lines transduced with an inducible sgLDLR vector in the presence or absence of Shield-1 (250 nM). Actin is used as a loading control.

**g.** Relative fold change in cell viability of control or SQLE-expressing DEL cell lines transduced with sgAAVS1 or sgLDLR after 5 days of growth.

**h.** Gene essentiality scores for untreated or cholesterol-supplemented Karpas299 cell line. Red dot denotes LDLR.

**i.** LDLR guide scores in Karpas299 cell lines expressing a control vector or SQLE cDNA in the presence or absence of cholesterol supplementation.

**j.** Coomassie blue staining of control IgG and LDLR monoclonal antibodies used in proliferation assays.

**k.** Relative fold change in cell viability of indicated cancer cell lines grown for 5 days in the presence of the indicated amounts of IgG or a monoclonal antibody against LDLR.

**l.** Relative fold change in cell viability of DEL cell lines transduced with a control vector or an SQLE cDNA grown for 5 days in the presence of the indicated amounts of IgG or an anti-LDLR monoclonal antibody compared to cells grown in the absence of both.

In **a**, **d**, **e**, **g**, **i**, **k** and **l** bars represent mean ± SD. For **a**, **e**, **g**, **i**, and **k**, $n = 3$ biologically independent samples. For **d** and **i**, $n = 5$ independent LDLR targeting sgRNAs. Statistical test used was two-tailed unpaired $t$-test.
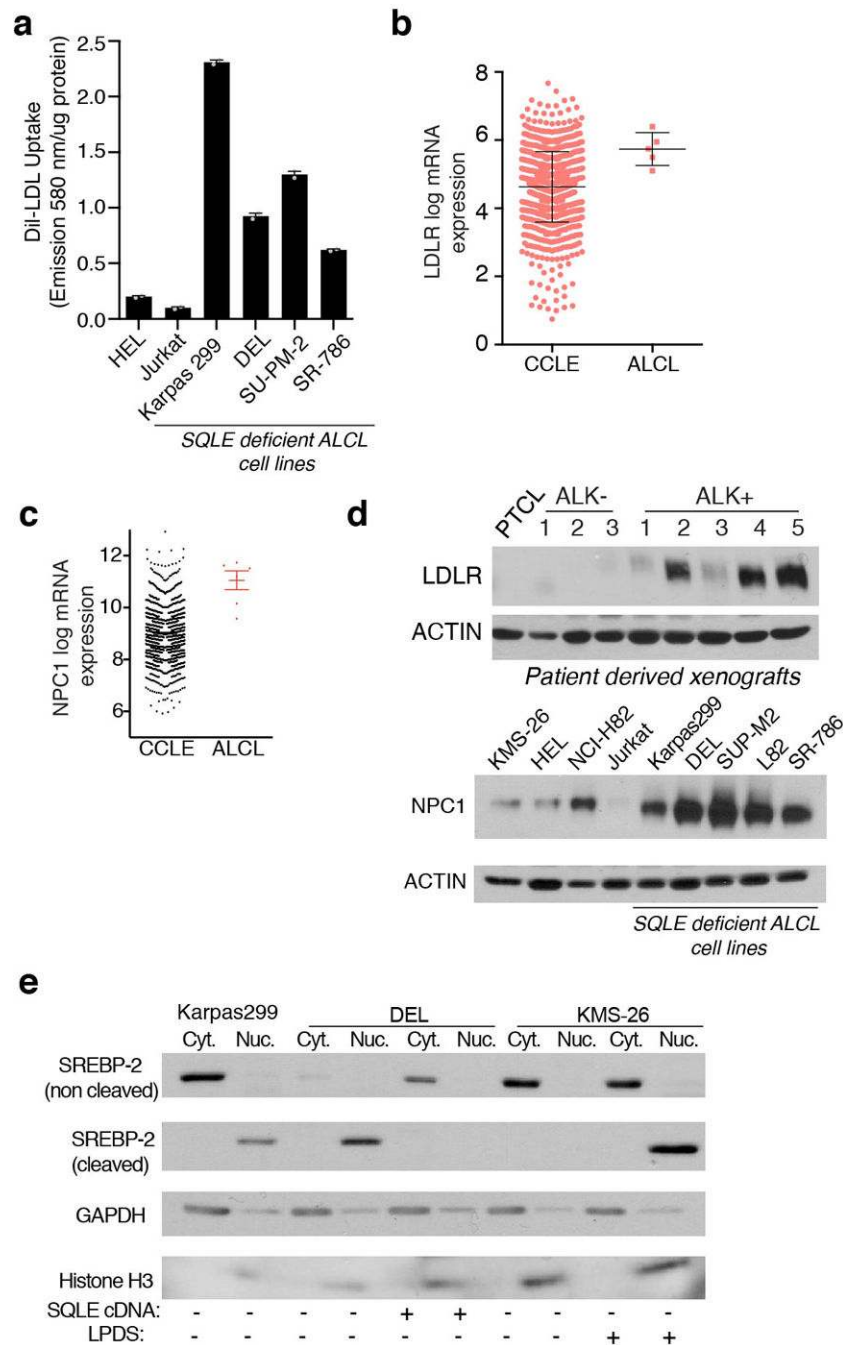
**Extended Data Figure 5. Upregulation of the LDL-cholesterol uptake pathway in ALK+ ALCLs**
**a.** Dil-LDL uptake in the indicated cell lines. Results were normalized to protein levels (mean ± SD, $n = 2$ biologically independent samples).
**b.** mRNA expression levels of LDLR (log) in cell lines from CCLE database compared to that of ALK+ ALCL lines (mean ± SD, $n = 1010$ independent cell lines for CCLE collection, 5 independent cell lines for ALCL).

**c.** Expression levels of Niemann-Pick C1 protein (NPC1) mRNA (log) in cell lines from CCLE database compared to that of ALK+ ALCL lines (mean ± SD, $n$ = 1010 independent cell lines for CCLE collection, 5 independent cell lines for ALCL).

**d.** Immunoblot of LDLR in the indicated primary patient derived xenografts (top). Immunoblotting of NPC1 in control and ALK+ ALCL cell lines (bottom). Actin is included as a loading control. PTCL: Peripheral T-cell Lymphoma.

**e.** Immunoblotting of SREBP-2 (non-cleaved and cleaved forms) in cytoplasmic and nuclear fractions of indicated cell lines expressing a vector or an SQLE cDNA. The cells were incubated for 24 hours in media containing either FBS (−) or LPDS (+). GAPDH and Histone H3 were used as cytoplasmic and nuclear loading controls respectively.
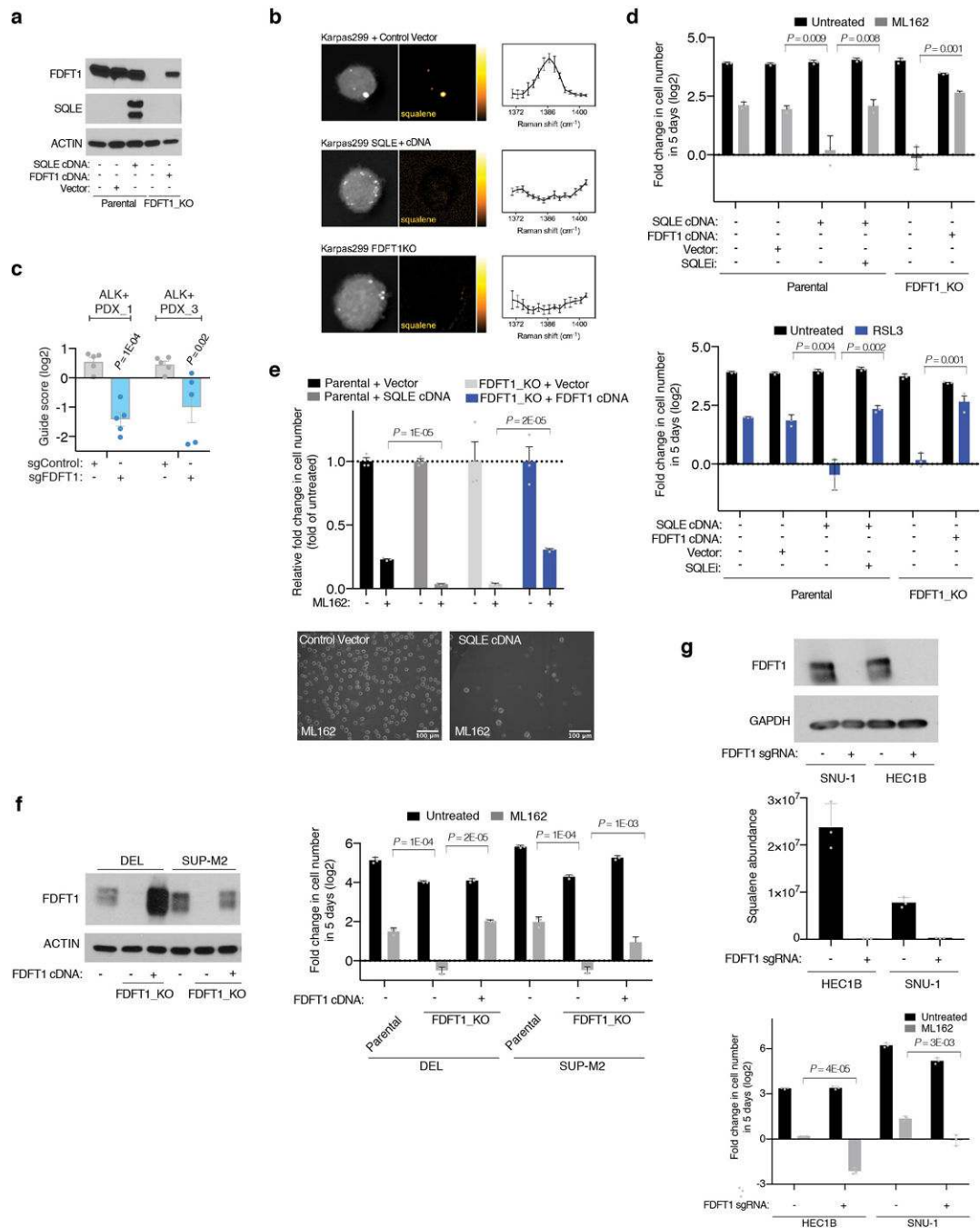
**Extended Data Figure 6. Squalene accumulation leads to resistance of SQLE-null cells to ferroptosis inducers**

**a.** Immunoblots of FDFT1 and SQLE in the indicated Karpas299 cell lines. Actin was used as the loading control.

**b.** Stimulated Raman scattering (SRS) imaging of squalene for indicated Karpas299 cells. Grey image shows cellular background ($1372 cm^{-1}$), squalene image (pseudo colored yellow hot, $1386 cm^{-1}$) (left). SRS spectra integrating intensity from lipid droplet with Raman peak

of squalene (1386cm$^{-1}$) (right) (mean ± SD, $n$ = 3 biologically independent samples). Error bar represent standard deviation from multiple lipid droplets in at least three cells.

**c.** sgRNA competition assay using a pool of five control (sgControl) and five FDFT1-targeting (sgFDFT1) sgRNAs in indicated patient derived xenografts. Transduced cells were injected subcutaneously to NOD/SCID gamma mice to generate tumors. Subsequent to 4 weeks of growth, genomic DNA was harvested to measure sgRNA abundance by deep sequencing. Average guide scores of tumors were calculated and graphed.

**d.** Relative fold change in cell viability of indicated Karpas299 lines treated with or without ML162 (20 nM, top) or RSL3 (30 nM, bottom) in the presence or absence of an SQLE inhibitor (1 uM) for 5 days.

**e.** Fold change in cell viability relative to untreated cells of indicated Karpas299 lines treated with or without ML162 (120 nM) for 2 days (top). Representative bright-field micrographs of indicated Karpas299 cells after 2 days of indicated treatments (bottom).

**f.** Immunoblotting of FDFT1 in the indicated DEL and SUP-M2 cell lines. Actin is used as a loading control (left). Relative fold change in cell viability of control, FDFT1-null and rescued DEL and SUP-M2 cell lines in the presence and absence of ML162 (20 nM) after 5 days,

**g.** Immunoblotting of FDFT1 in the indicated HEC1B and SNU-1 cell lines. Actin is used as a loading control (top). Squalene abundance of the indicated cell lines (middle). Relative fold change in cell viability of control and FDFT1-null HEC1B and SNU-1 cell lines in the presence and absence of ML162 (200 nM for HEC1B lines, 1 uM for SNU-1 cell lines) and grown for 5 days.

In **c**, **d**, **e**, **f** and **g** bars represent mean ± SD. For **c**, $n$ = 5 independent sgRNAs targeting a control region or LDLR gene. For **d**, **e**, **f**, and **g**, $n$ = 3 biologically independent samples. Statistical test used was two-tailed unpaired $t$-test.

**a**



**b**



**c**



**d**
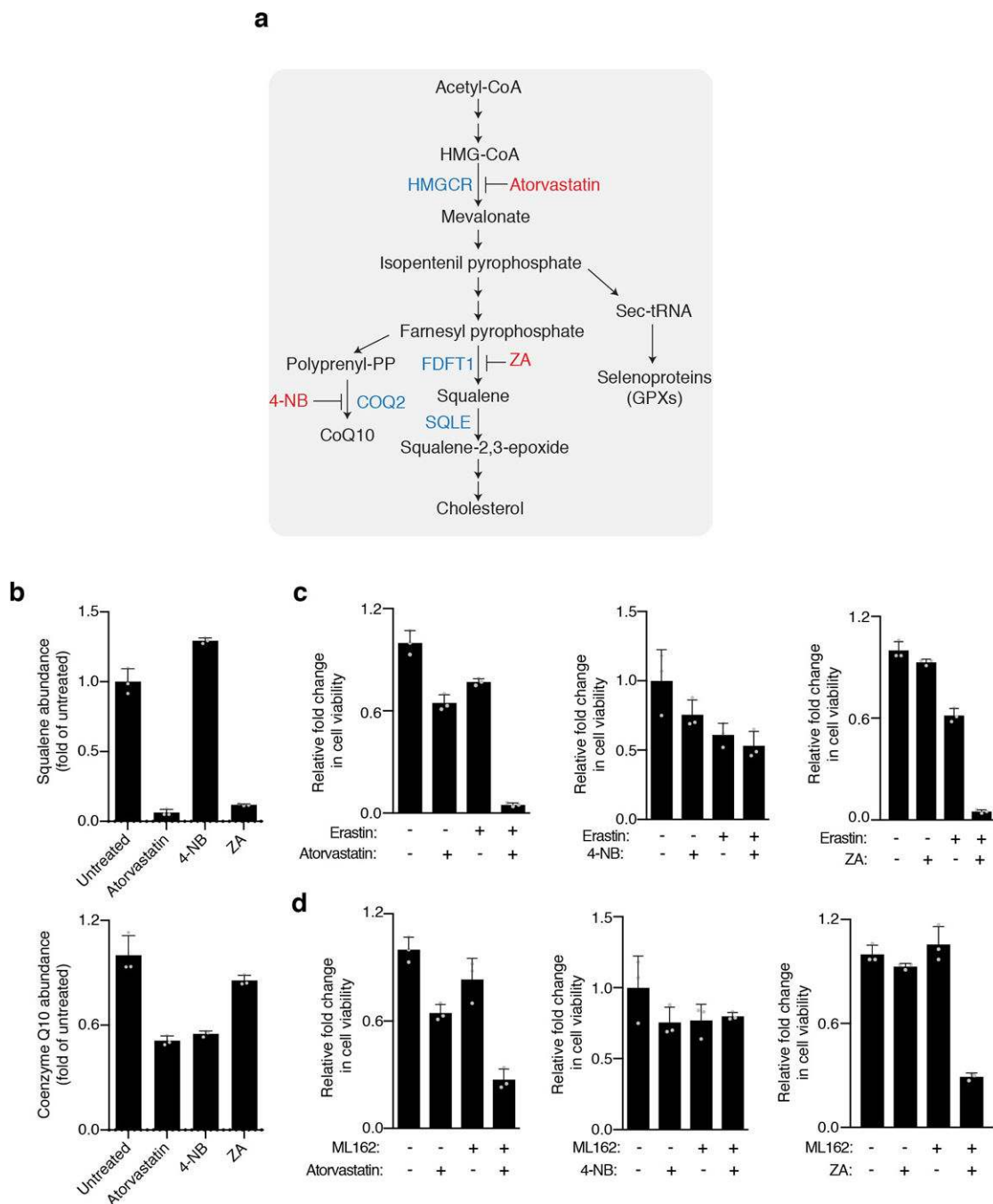


**Extended Data Figure 7. Blocking squalene accumulastion sensitizes ALCLs to a GPX4 inhibitor (ML162) and erastin**

**a.** Mevalonate pathway in mammalian cells and fates of the side reactions. Reactions catalyzed by HMGCR, COQ2, FDFT1 and SQLE, and chemical inhibitors of these enzymes, are indicated.

**b.** Relative abundance of squalene and coenzyme Q10 in Karpas299 treated for 24 hrs with atorvastatin (1 uM), 4-nitrobenzoate (4-NB, 1 mM) or zaragozic acid (ZA, 20 uM) to untreated.

**c.** Relative fold change in cell viability of Karpas299 cells treated with erastin (1 uM), atorvastatin (1 uM), 4-nitrobenzoate (4-NB, 1 mM), zaragozic acid (ZA, 20 uM) or a combination of two of them after 5 days to untreated.

**d.** Relative fold change in cell viability compared to untreated cells of Karpas299 cells treated with ML162 (25 nM), atorvastatin (1 uM), 4-nitrobenzoate (4-NB, 1 mM), zaragozic acid (ZA, 20 uM) or a combination of two of them after 5 days.

In **b**, **c** and **d** bars represent mean ± SD. For **b**, **c** and **d**, $n = 3$ biologically independent samples.
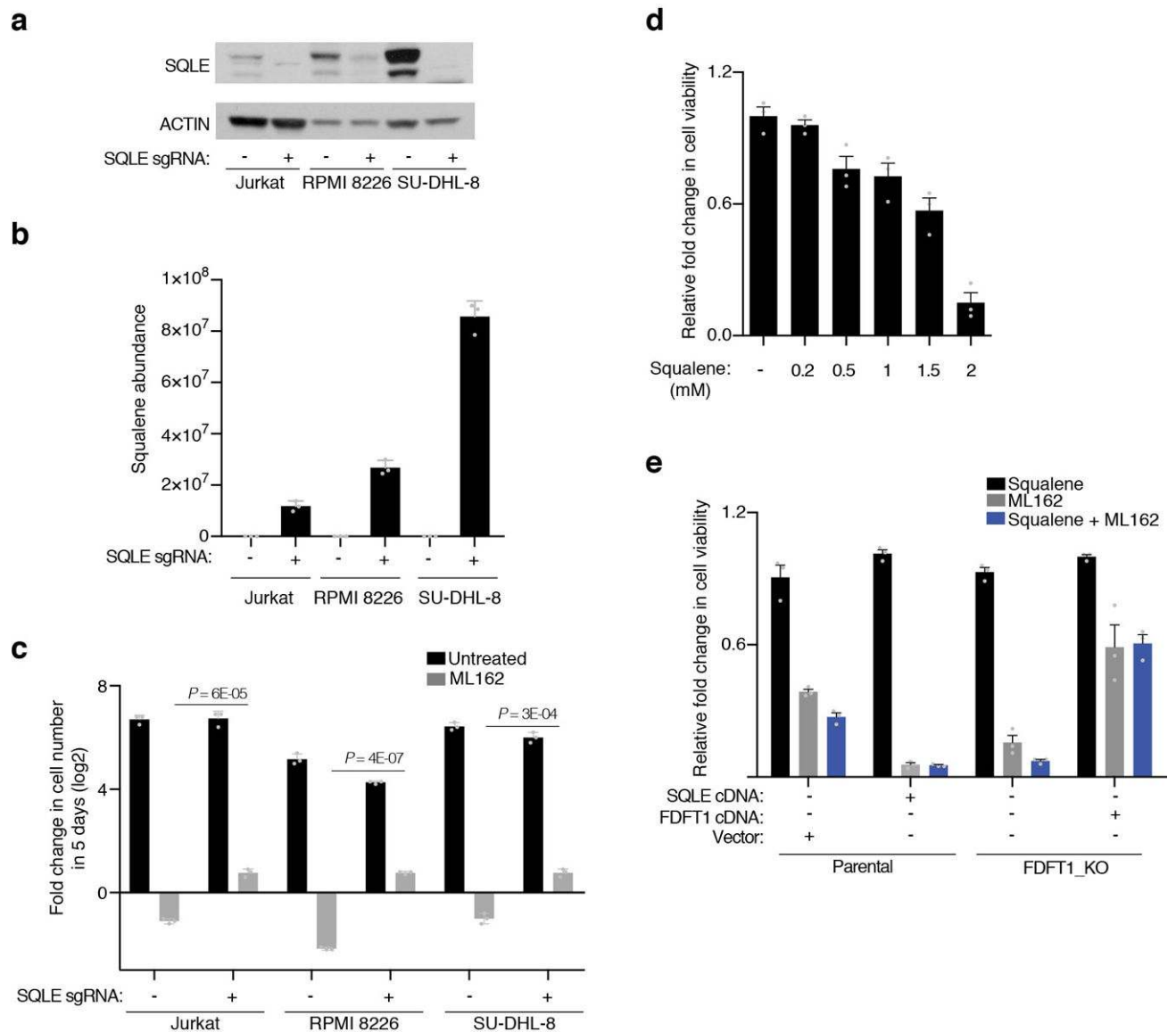


**Extended Data Figure 8. Loss of SQLE decreases sensitivity of cancer cell lines to ferroptosis inducers**

**a.** Immunoblotting of SQLE in the indicated cell lines transduced with a vector or sgSQLE. Actin is used as a loading control.

**b.** Squalene abundance in the indicated cell lines.

**c.** Relative fold change in cell viability of control and sgSQLE-expressing cell lines in the presence and absence of ML162 (500 nM for Jurkat lines, 200 nM for RPMI 8226 and SU-DHL-8 cell lines) grown for 5 days.

**d.** Relative fold change in cell viability of Karpas299 parental cells supplemented with the indicated concentrations of exogenous squalene to untreated cells.

**e.** Relative fold change in cell viability of Karpas299 parental or FDFT1 null cells expressing a vector, SQLE cDNA or FDFT1 cDNA treated with or without ML162, squalene or both, to untreated cells.

In **b**, **c**, **d** and **e** bars represent mean ± SD. For **b**, **c**, **d** and **e**, $n = 3$ biologically independent samples. Statistical test used was two-tailed unpaired $t$-test.
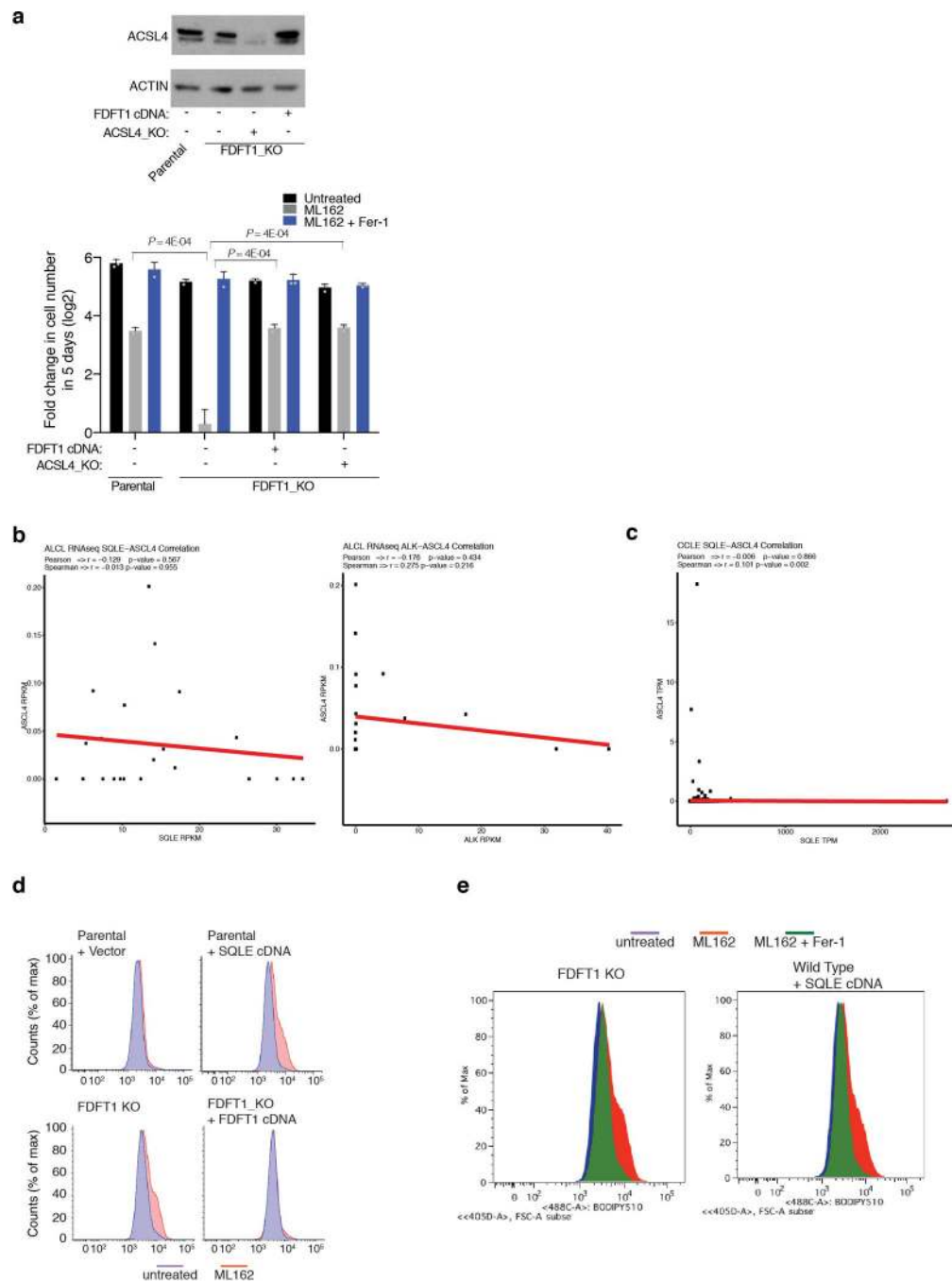
**Extended Data Figure 9. Inhibition of PUFA synthesis prevents ferroptotic cell death in ALCLs**
**a.** Immunoblotting of ACSL4 in the indicated Karpas299 cells. Actin is used as a loading control (top). Relative fold change in cell viability of indicated Karpas299 cell lines in the presence or absence of ML162 (20 nM) and Fer-1 (1 uM) for 5 days (bottom) (mean ± SD, $n$ = 3 biologically independent samples). Statistics: two-tailed unpaired $t$-test.
**b.** Correlation of mRNA levels of ACSL4 with SQLE (left) and ALK (right) in primary ALCLs dataset ($n$ = 22 biologically independent samples).

**c.** Correlation of mRNA levels of ACSL4 with SQLE in CCLE dataset ($n$ = 935 independent cell lines).

**d.** Lipid peroxidation assessed by flow cytometry measuring C11-BODIPY fluorescence of indicated Karpas299 cell lines after an 18 hr treatment with ML162 (200 nM). Representative data from one of three experiments is shown.

**e.** Lipid peroxidation assessed by flow cytometry measuring C11-BODIPY fluorescence of indicated Karpas299 cell lines after an 18 hr treatment in the presence and absence of ML162 (200 nM) and Fer-1 (1 uM).
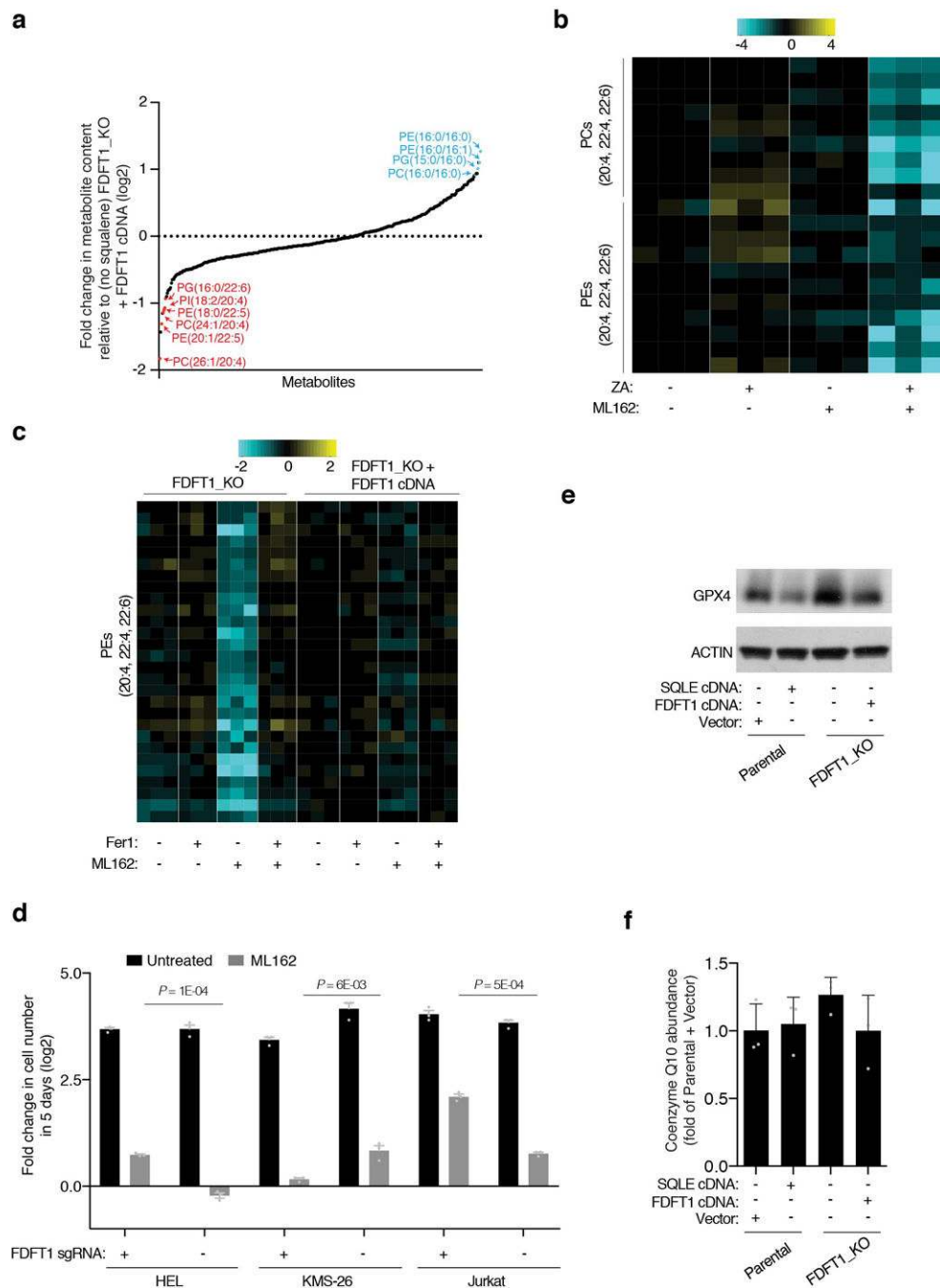
**Extended Data Figure 10. Squalene accumulation rewires membrane phospholipid composition**
**a.** Unbiased lipidomic analysis of Karpas299 FDFT1-null cell line relative to its rescued isogenic counterpart expressing FDFT1 cDNA. Fold change ($\log_2$) in metabolite abundance was graphed and membrane phospholipids containing saturated and polyunsaturated fatty acids are indicated.
**b.** Heat map showing fold changes ($\log_2$) in indicated phosphatidylcholines (PCs) and phosphatidylethanolamines (PEs) of Karpas299 cells cultured for 24 hours in the absence or

presence of ZA (zaragozic acid, 20 uM) and ML162 (200 nM) relative to untreated cells. Triplicates of each condition are shown. Color bar indicates $\log_2$ change in abundance.

**c.** Heat map showing fold changes ($\log_2$) in indicated phosphatidylethanolamines (PEs) of indicated Karpas299 cell lines cultured for 24 hours with Fer-1 (1 uM) and ML162 (200 nM). Triplicates of each condition are shown. Color bar indicates $\log_2$ change in abundance.

**d.** Relative fold change in cell viability of HEL, KMS-26 and Jurkat cell lines expressing vector or an sgRNA targeting FDFT1 in the presence or absence of ML162 (20 nM) for 5 days.

**e.** Immunoblotting of GPX4 in indicated Karpas299 cell lines expressing a vector, SQLE cDNA, FDFT1 cDNA or an sgRNA targeting FDFT1. Actin is used as a loading control.

**f.** Coenzyme Q10 abundance of indicated Karpas299 cell lines relative to parental cells expressing a control vector.

In **d** and **f** bars represent mean ± SD. For **d** and **f**, $n = 3$ biologically independent samples. Statistical test used was two-tailed unpaired $t$-test.

## Supplementary Material

Refer to Web version on PubMed Central for supplementary material.

## ACKNOWLEDGEMENTS

## REFERENCES

1. Goldstein JL & Brown MS Regulation of the mevalonate pathway. Nature 343, 425–430, doi: 10.1038/343425a0 (1990). [PubMed: 1967820]

2. Delage B et al. Arginine deprivation and argininosuccinate synthetase expression in the treatment of cancer. Int J Cancer 126, 2762–2772, doi:10.1002/ijc.25202 (2010). [PubMed: 20104527]

3. Kidd JG Regression of transplanted lymphomas induced in vivo by means of normal guinea pig serum. II. Studies on the nature of the active serum constituent: histological mechanism of the regression: tests for effects of guinea pig serum on lymphoma cells in vitro: discussion. J Exp Med 98, 583–606 (1953). [PubMed: 13109111]

4. Letouze E et al. SDH mutations establish a hypermethylator phenotype in paraganglioma. Cancer Cell 23, 739–752, doi:10.1016/j.ccr.2013.04.018 (2013). [PubMed: 23707781]

5. Lu C & Thompson CB Metabolic regulation of epigenetics. Cell Metab 16, 9–17, doi:10.1016/j.cmet.2012.06.001 (2012). [PubMed: 22768835]

6. Xu W et al. Oncometabolite 2-hydroxyglutarate is a competitive inhibitor of alpha-ketoglutarate-dependent dioxygenases. Cancer Cell 19, 17–30, doi:10.1016/j.ccr.2010.12.014 (2011). [PubMed: 21251613]

7. Esfahani M, Scerbo L & Devlin TM A requirement for cholesterol and its structural features for a human macrophage-like cell line. J Cell Biochem 25, 87–97, doi:10.1002/jcb.240250204 (1984). [PubMed: 6480716]

8. Villa GR et al. An LXR-Cholesterol Axis Creates a Metabolic Co-Dependency for Brain Cancers. Cancer Cell 30, 683–693, doi:10.1016/j.ccell.2016.09.008 (2016). [PubMed: 27746144]

9. Brown MS, Kovanen PT & Goldstein JL Regulation of plasma cholesterol by lipoprotein receptors. Science 212, 628–635 (1981). [PubMed: 6261329]

10. Calleros L, Sanchez-Hernandez I, Baquero P, Toro MJ & Chiloeches A Oncogenic Ras, but not (V600E)B-RAF, protects from cholesterol depletion-induced apoptosis through the PI3K/AKT pathway in colorectal cancer cells. Carcinogenesis 30, 1670–1677, doi:10.1093/carcin/bgp188 (2009). [PubMed: 19700418]

11. Gill S, Stevenson J, Kristiana I & Brown AJ Cholesterol-dependent degradation of squalene monooxygenase, a control point in cholesterol synthesis beyond HMG-CoA reductase. Cell Metab 13, 260–273, doi:10.1016/j.cmet.2011.01.015 (2011). [PubMed: 21356516]

12. Crescenzo R et al. Convergent mutations and kinase fusions lead to oncogenic STAT3 activation in anaplastic large cell lymphoma. Cancer Cell 27, 516–532, doi:10.1016/j.ccell.2015.03.006 (2015). [PubMed: 25873174]

13. Sullivan LB, Gui DY & Heiden MGV Altered metabolite levels in cancer: implications for tumour biology and cancer therapy. Nat Rev Cancer 16, 680–693, doi:10.1038/nrc.2016.85 (2016). [PubMed: 27658530]

14. Finotti E, D'Ambrosio M, Paoletti F, Vivanti V & Quaglia G Synergistic effects of alpha-tocopherol, beta-sitosterol and squalene on antioxidant activity assayed by crocin bleaching method. Nahrung 44, 373–374, doi:10.1002/1521-3803(20001001)44:5<373::AID-FOOD373>3.0.CO;2-0 (2000). [PubMed: 11075383]

15. Huang ZR, Lin YK & Fang JY Biological and pharmacological activities of squalene and related compounds: potential uses in cosmetic dermatology. Molecules 14, 540–554, doi:10.3390/molecules14010540 (2009). [PubMed: 19169201]

16. Dixon SJ et al. Ferroptosis: an iron-dependent form of nonapoptotic cell death. Cell 149, 1060–1072, doi:10.1016/j.cell.2012.03.042 (2012). [PubMed: 22632970]

17. Friedmann Angeli JP et al. Inactivation of the ferroptosis regulator Gpx4 triggers acute renal failure in mice. Nat Cell Biol 16, 1180–1191, doi:10.1038/ncb3064 (2014). [PubMed: 25402683]

18. Yang WS et al. Regulation of ferroptotic cancer cell death by GPX4. Cell 156, 317–331, doi:10.1016/j.cell.2013.12.010 (2014). [PubMed: 24439385]

19. Kagan VE et al. Oxidized arachidonic and adrenic PEs navigate cells to ferroptosis. Nat Chem Biol 13, 81–90, doi:10.1038/nchembio.2238 (2017). [PubMed: 27842066]

20. Shimada K et al. Global survey of cell death mechanisms reveals metabolic regulation of ferroptosis. Nat Chem Biol 12, 497–503, doi:10.1038/nchembio.2079 (2016). [PubMed: 27159577]

21. Viswanathan VS et al. Dependency of a therapy-resistant state of cancer cells on a lipid peroxidase pathway. Nature 547, 453–457, doi:10.1038/nature23007 (2017). [PubMed: 28678785]

22. Isaacs JS et al. HIF overexpression correlates with biallelic loss of fumarate hydratase in renal cancer: novel role of fumarate in regulation of HIF stability. Cancer Cell 8, 143–153, doi:10.1016/j.ccr.2005.06.017 (2005). [PubMed: 16098467]

23. Pollard PJ et al. Targeted inactivation of fh1 causes proliferative renal cyst development and activation of the hypoxia pathway. Cancer Cell 11, 311–319, doi:10.1016/j.ccr.2007.02.005 (2007). [PubMed: 17418408]

24. Romero R et al. Keap1 loss promotes Kras-driven lung cancer and results in dependence on glutaminolysis. Nat Med 23, 1362–1368, doi:10.1038/nm.4407 (2017). [PubMed: 28967920]

25. Hangauer MJ et al. Drug-tolerant persister cancer cells are vulnerable to GPX4 inhibition. Nature 551, 247–250, doi:10.1038/nature24297 (2017). [PubMed: 29088702]

26. Piskounova E et al. Oxidative stress inhibits distant metastasis by human melanoma cells. Nature 527, 186–191, doi:10.1038/nature15726 (2015). [PubMed: 26466563]

27. Alvarez SW et al. NFS1 undergoes positive selection in lung tumours and protects cells from ferroptosis. Nature 551, 639–643, doi:10.1038/nature24637 (2017). [PubMed: 29168506]

28. Gambacorti Passerini C. et al. Crizotinib in advanced, chemoresistant anaplastic lymphoma kinase-positive lymphoma patients. J Natl Cancer Inst 106, djt378, doi:10.1093/jnci/djt378 (2014). [PubMed: 24491302]

29. Senturk S et al. Rapid and tunable method to temporally control gene editing based on conditional Cas9 stabilization. Nat Commun 8, 14370, doi:10.1038/ncomms14370 (2017). [PubMed: 28224990]

30. Ambrogio C et al. NPM-ALK oncogenic tyrosine kinase controls T-cell identity by transcriptional regulation and epigenetic silencing in lymphoma cells. Cancer Res 69, 8611–8619, doi: 10.1158/0008-5472.CAN-09-2655 (2009). [PubMed: 19887607]

31. Hu C et al. RPLC-ion-trap-FTMS method for lipid profiling of plasma: method validation and application to p53 mutant mouse model. J Proteome Res 7, 4982–4991, doi:10.1021/pr800373m (2008). [PubMed: 18841877]

32. Bird SS, Marur VR, Sniatynski MJ, Greenberg HK & Kristal BS Serum lipidomics profiling using LC-MS and high-energy collisional dissociation fragmentation: focus on triglyceride detection and characterization. Anal Chem 83, 6648–6657, doi:10.1021/ac201195d (2011). [PubMed: 21774539]

33. Taguchi R & Ishikawa M Precise and global identification of phospholipid molecular species by an Orbitrap mass spectrometer and automated search engine Lipid Search. J Chromatogr A 1217, 4229–4239, doi:10.1016/j.chroma.2010.04.034 (2010). [PubMed: 20452604]

34. Yamada T et al. Development of a lipid profiling system using reverse-phase liquid chromatography coupled to high-resolution mass spectrometry with rapid polarity switching and an automated lipid identification software. J Chromatogr A 1292, 211–218, doi:10.1016/j.chroma. 2013.01.078 (2013). [PubMed: 23411146]

35. Birsoy K et al. Metabolic determinants of cancer cell sensitivity to glucose limitation and biguanides. Nature 508, 108–112, doi:10.1038/nature13110 (2014). [PubMed: 24670634]

36. Krueger F & Andrews SR Bismark: a flexible aligner and methylation caller for Bisulfite-Seq applications. Bioinformatics 27, 1571–1572, doi:10.1093/bioinformatics/btr167 (2011). [PubMed: 21493656]

37. Nguyen AT, Hirama T, Chauhan V, Mackenzie R & Milne R Binding characteristics of a panel of monoclonal antibodies against the ligand binding domain of the human LDLr. J Lipid Res 47, 1399–1405, doi:10.1194/jlr.M600130-JLR200 (2006). [PubMed: 16601300]

38. Freudiger CW et al. Label-free biomedical imaging with high sensitivity by stimulated Raman scattering microscopy. Science 322, 1857–1861, doi:10.1126/science.1165758 (2008). [PubMed: 19095943]

39. Barretina J et al. The Cancer Cell Line Encyclopedia enables predictive modelling of anticancer drug sensitivity. Nature 483, 603–607, doi:10.1038/nature11003 (2012). [PubMed: 22460905]

40. Cheng M et al. CEP-28122, a highly potent and selective orally active inhibitor of anaplastic lymphoma kinase with antitumor activity in experimental models of human cancers. Mol Cancer Ther 11, 670–679, doi:10.1158/1535-7163.MCT-11-0776 (2012). [PubMed: 22203728]
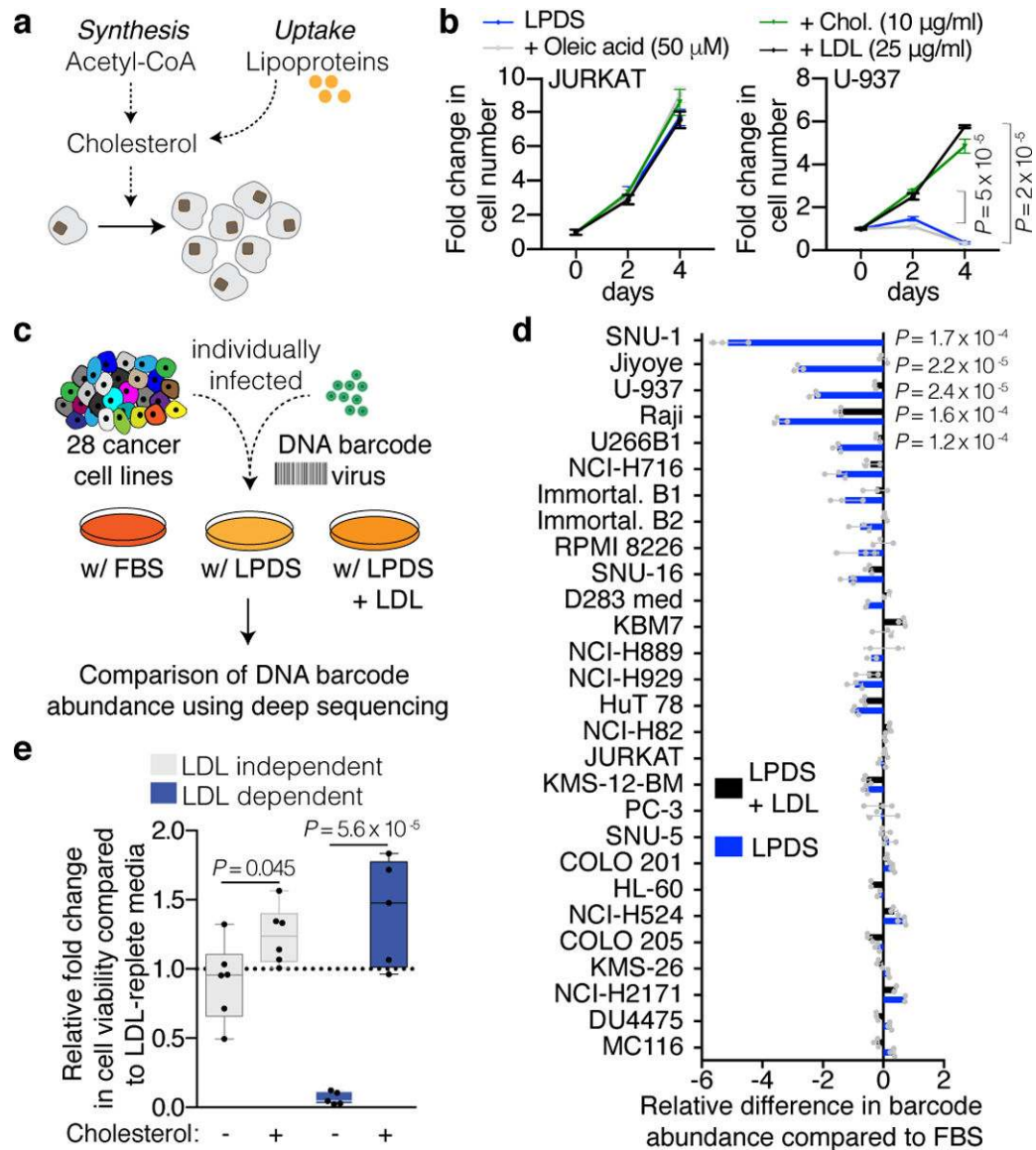
**Figure 1. Identification of cholesterol auxotrophic cancer cell lines using a barcode-based competition assay**

**a.** Cholesterol metabolism in mammalian cells.

**b.** Fold change in cell number of Jurkat and U-937 cells cultured with the indicated concentrations of cholesterol, LDL, and oleic acid.

**c.** Experimental design outline of cell competition assay. 28 cancer cell lines were barcoded with individual DNA barcodes and cultured for 2 weeks in media supplemented with FBS, LPDS, or LPDS/LDL (25ug/ml). FBS, Fetal Bovine Serum; LPDS, lipoprotein depleted serum; LDL, low density lipoprotein.

**d.** Relative difference in barcode abundance of indicated cell lines in the competition assay grown under LPDS-supplemented media with (black) and without (blue) LDL, relative to FBS.

**e.** Relative fold change in cell number of LDL independent (gray) and dependent (blue) cell lines in the presence or absence of cholesterol.

In **b** and **d**, bars represent mean ± SD. In **e**, the boxes represent the median, and the first and third quartiles, and the whiskers represent the minimum and maximum of all data points. For **b**, $n = 3$ biologically independent samples. For **d**, $n = 3$ independent barcodes per cell line. For **e**, $n = 5–6$ biologically independent cell lines. Statistical test used was two-tailed unpaired *t*-test.
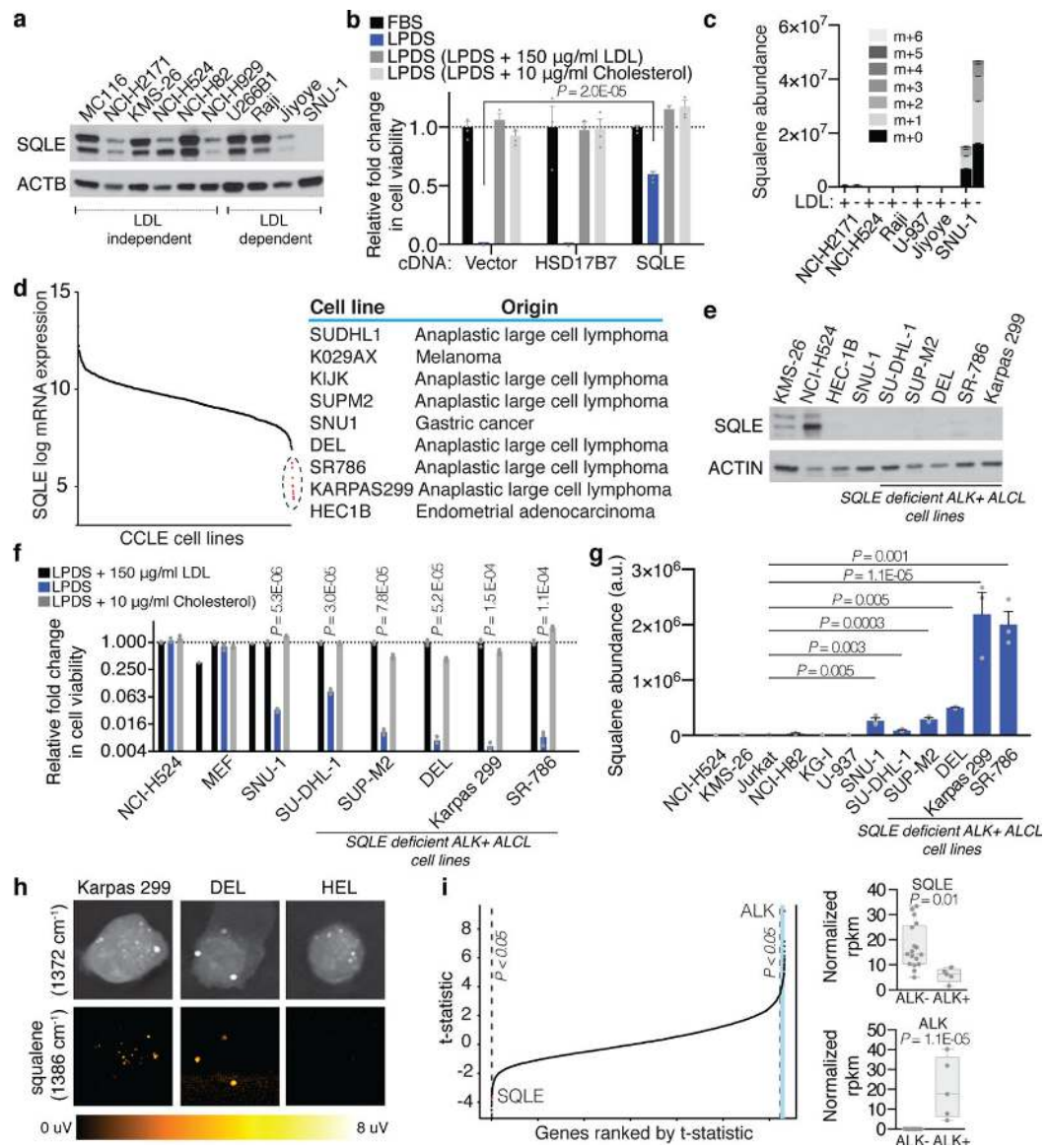
**Figure 2. ALK+ ALCLs are auxotrophic for cholesterol due to lack of SQLE expression**

**a.** Immunoblotting for SQLE in LDL-dependent and independent cancer cell lines. Actin was used as a loading control.

**b.** Relative fold change in cell viability of control and SQLE or HSD217B7 expressing SNU-1 cancer cells grown for 5 days under LPDS in the absence or presence of LDL or cholesterol.

**c.** Mass isotopomer analysis of squalene in indicated cancer cell lines in the presence or absence of LDL after a 24 hour incubation with [U-$^{13}$C]-Acetate.

**d.** Expression levels of SQLE mRNA in 1037 cell lines from CCLE database. Cell lines with undetectable SQLE mRNA levels and their tissue origins are indicated.

**e.** Immunoblotting for SQLE in ALK+ ALCL and control cancer cell lines. Actin was used as the loading control.

**f.** Relative fold change in cell viability of indicated cancer cell lines grown for 5 days with LPDS in the absence and presence of LDL or cholesterol.

**g.** Squalene abundance in control and SQLE deficient cancer cell lines.

**h.** Raman spectra of squalene and cholesterol for the indicated cell lines. SRS images were obtained at squalene channel ($1386 cm^{-1}$) and at lipid channel ($1372 cm^{-1}$) in the same cell.

**i.** Genes ranked by differential expression analysis of primary ALK+ ALCL primary samples compared to ALK- samples (left). Student t-test statistic of each gene was ranked as a function of its t-test rank. ALK- and ALK+ normalized expression (fpkm) of SQLE and ALK are indicated (right).

In **b**, **c**, **f** and **g**, bars represent mean ± SD. In **i**, the boxes represent the median, and the first and third quartiles, and the whiskers represent the minimum and maximum of all data points. For **b**, **c**, **f** and **g,** $n = 3$ biologically independent samples. For **i**, $n = 17$ biologically independent ALK- samples, 5 biologically independent ALK+ samples. Statistical test used was two-tailed unpaired *t*-test.
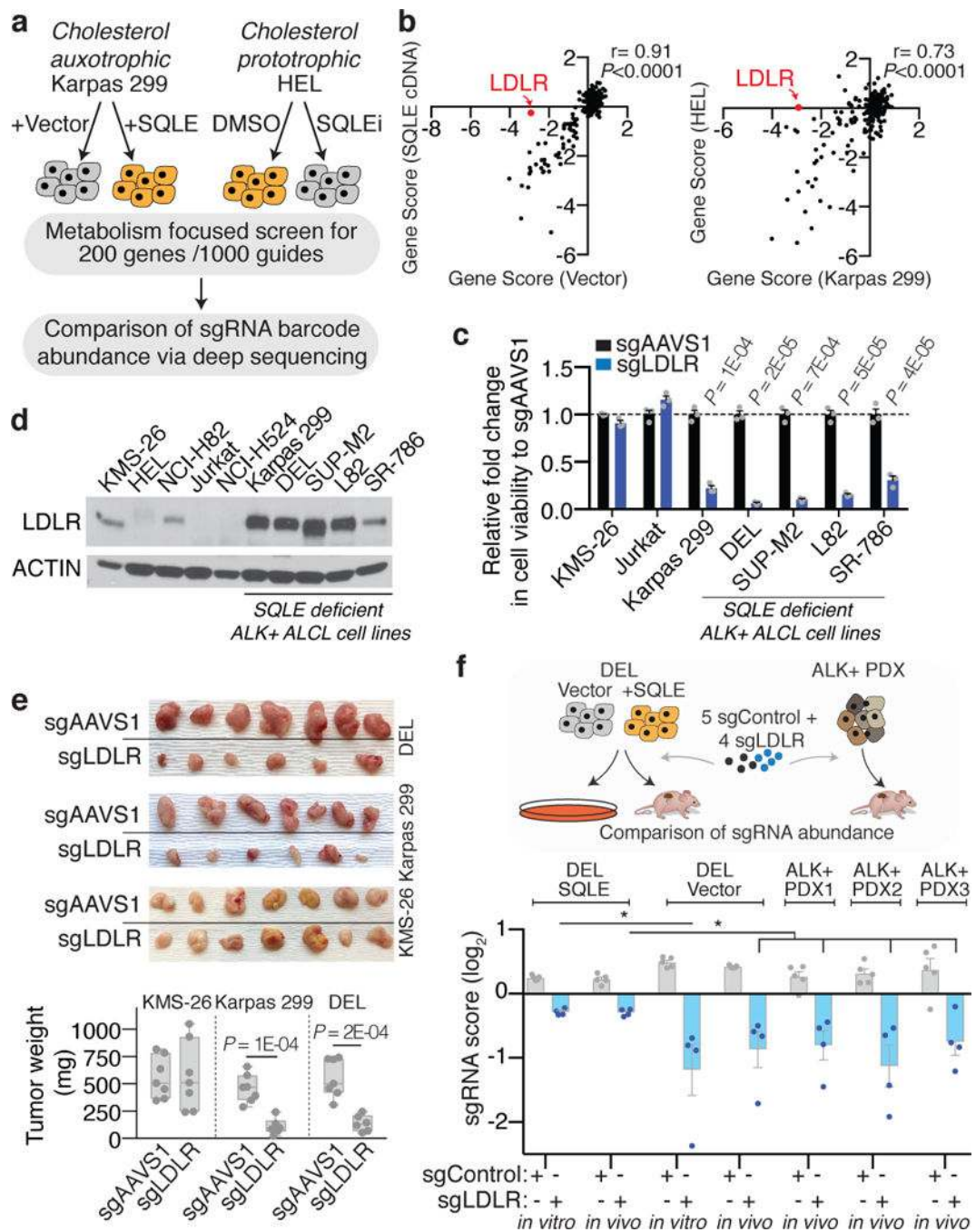


**Figure 3. In ALK+ ALCLs LDLR is upregulated and is a potential therapeutic target**

**a.** Schematic for CRISPR-Cas9 based negative selection screening.

**b.** Comparison of gene essentiality between indicated cancer cell lines. Pearson correlation coefficients are indicated. Red dot denotes LDLR.

**c.** Relative fold change in cell viability of indicated cancer cell lines infected with sgAAVS1 or sgLDLR and grown for 5 days.

**d.** Immunoblot of LDLR in the indicated cancer cell lines. Actin was used as the loading control.

**e.** Representative images (top) and weights (bottom) of subcutaneous tumour xenografts derived from indicated cancer lines expressing sgRNAs targeting AAVS or LDLR after 4 weeks of growth.

**f.** Mini sgRNA competition assay using a pool of control (sgControl) and LDLR-targeting (sgLDLR) sgRNAs in indicated cancer cell lines and patient derived xenografts. Average guide scores of tumors and cell lines were calculated and graphed. (* $p < 0.05$). PDX: Patient derived xenograft.

In **c** and **f**, bars represent mean ± SD. In **e**, the boxes represent the median, and the first and third quartiles, and the whiskers represent the minimum and maximum of all data points. For **c**, $n = 3$ biologically independent samples. For **e**, $n = 6$–7 biologically independent samples. For **f**, $n = 5$ independent sgRNAs targeting a control region and 4 sgRNAs targeting LDLR gene. Statistical test used was two-tailed unpaired $t$-test.
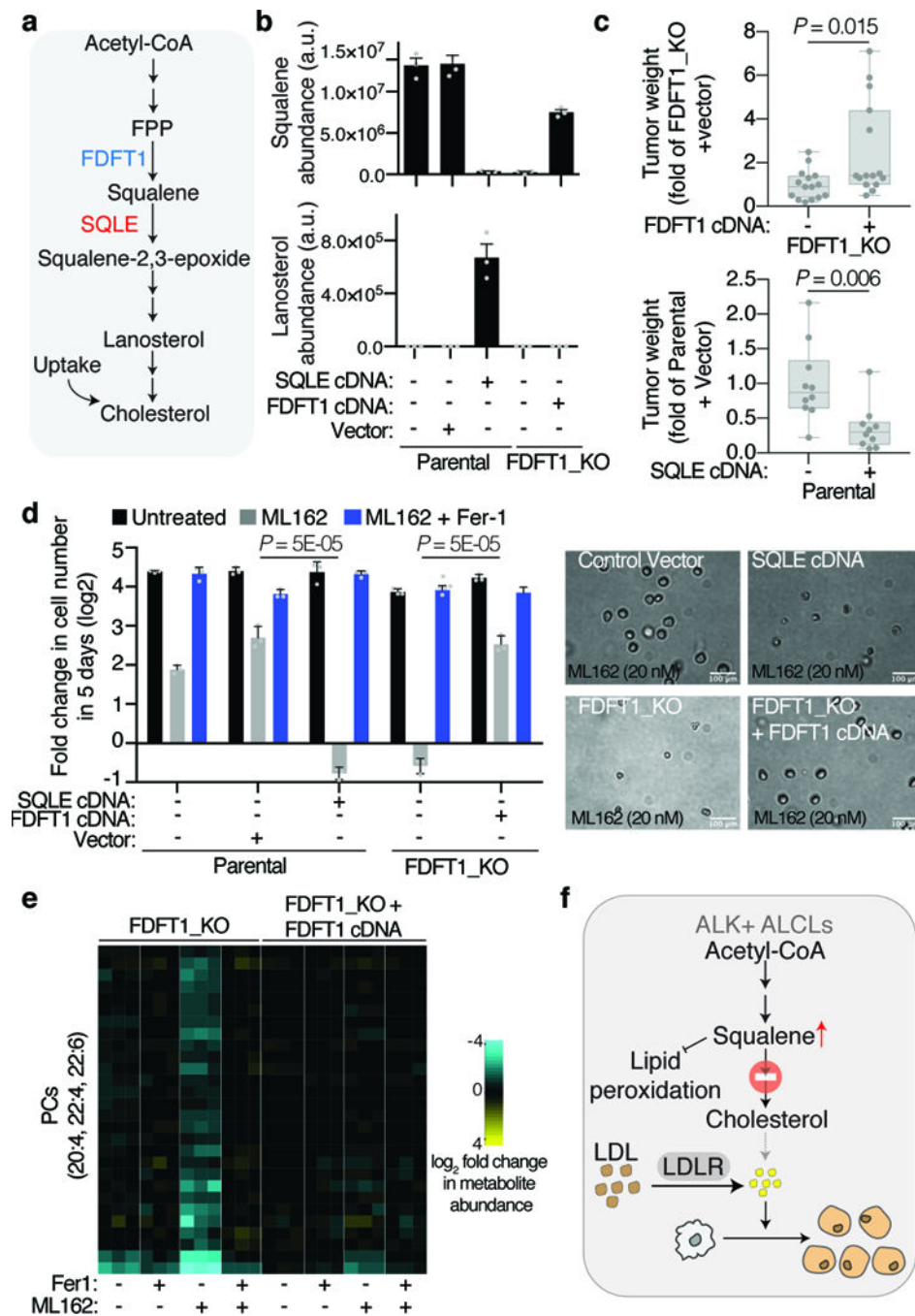
**Figure 4. Squalene accumulation rewires membrane lipid composition and protects ALCLs from ferroptosis**

**a.** Metabolic reactions catalyzed by FDFT1 and SQLE in the cholesterol synthesis pathway.

**b.** Squalene and lanosterol abundance in indicated Karpas299 cell lines.

**c.** Relative fold change in tumor weight of indicated Karpas299 derived xenografts.

**d.** Relative fold change in cell viability of indicated Karpas299 cells in the absence and presence of ML162 (20 nM) and Fer-1 (1 uM) for 5 days (left). Representative bright-field micrographs of indicated Karpas299 cells after treatment (right).

**e.** Heat map showing fold changes (log$_2$) in PUFA containing phosphatidylcholines (PCs) of indicated Karpas299 cell lines after incubation with Fer-1 (1 uM) and ML162 (200 nM) for 24 hours.

**f.** Model depicting how loss of SQLE expression results in cholesterol auxotrophy and the accumulation of squalene in ALCLs. Excess squalene may in turn protect ALCLs from lipid peroxidation damage.

In **b** and **d**, bars represent mean ± SD. In **c**, the boxes represent the median, and the first and third quartiles, and the whiskers represent the minimum and maximum of all data points. For **b** and **d,** $n = 3$ biologically independent samples. For **c**, $n = 10$–15 biologically independent samples. Statistical test used was two-tailed unpaired $t$-test.